CellPress

Neuron
Article

Sleep and Movement Differentiates Actions of Two Types of Somatostatin-Expressing GABAergic Interneuron in Rat Hippocampus

Linda Katona,[1,*] Damien Lapray,[1,4] Tim J. Viney,[1] Abderrahim Oulhaj,[2] Zsolt Borhegyi,[3] Benjamin R. Micklem,[1] Thomas Klausberger,[1,3,*] and Peter Somogyi[1,3,*]

[1]MRC Anatomical Neuropharmacology Unit, Department of Pharmacology, University of Oxford, Mansfield Road, Oxford, OX1 3TH, UK
[2]Institute of Public Health, College of Medicine and Health Sciences, United Arab Emirates University, Al-Ain, P.O. Box 17666, United Arab Emirates
[3]Center for Brain Research, Medical University of Vienna, Spitalgasse 4, Vienna, A-1090, Austria
[4]Present address: Brain Mind Institute, School of Life Sciences, École Polytechnique Fédérale de Lausanne, SV 2805, Station 19, Lausanne, CH-1015, Switzerland
*Correspondence: linda.katona@pharm.ox.ac.uk (L.K.), thomas.klausberger@meduniwien.ac.at (T.K.), peter.somogyi@pharm.ox.ac.uk (P.S.)
http://dx.doi.org/10.1016/j.neuron.2014.04.007
This is an open access article under the CC BY-NC-ND license (http://creativecommons.org/licenses/by-nc-nd/3.0/).

SUMMARY

Neuropeptides acting on pre- and postsynaptic receptors are coreleased with GABA by interneurons including bistratified and O-LM cells, both expressing somatostatin but innervating segregated dendritic domains of pyramidal cells. Neuropeptide release requires high-frequency action potentials, but the firing patterns of most peptide/GABA-releasing interneurons during behavior are unknown. We show that behavioral and network states differentiate the activities of bistratified and O-LM cells in freely moving rats. Bistratified cells fire at higher rates during sleep than O-LM cells and, unlike O-LM cells, strongly increase spiking during sharp wave-associated ripples (SWRs). In contrast, O-LM interneurons decrease firing during sleep relative to awake states and are mostly inhibited during SWRs. During movement, both cell types fire cooperatively at the troughs of theta oscillations but with different frequencies. Somatostatin and GABA are differentially released to distinct dendritic zones of CA1 pyramidal cells during sleep and wakefulness to coordinate segregated glutamatergic inputs from entorhinal cortex and CA3.

INTRODUCTION

Somatostatin (SOM) is a 14 amino acid neuropeptide originally identified as somatotropin release-inhibiting factor in the hypothalamus (Brazeau et al., 1973). It is distributed widely in the brain and is coreleased with amino acid neurotransmitters. Under normal conditions, SOM is exclusively expressed in cortical GABAergic interneurons (Somogyi et al., 1984). In the hippocampal CA1 area, at least five distinct neuron types express SOM (Baude et al., 1993; Chittajallu et al., 2013; Katona et al., 1999; Klausberger et al., 2004) and some SOM-expressing GABAergic cell types also project to extrahippocampal areas (Gulyás et al., 2003; Jinno et al., 2007), including the entorhinal cortex in the mouse (Melzer et al., 2012). All of these neurons probably release SOM and GABA within the dendritic domain of pyramidal cells and also innervate other interneurons (Gulyás et al., 2003; Jinno et al., 2007; Katona et al., 1999). Some interneurons, including the bistratified cells, also express neuropeptide tyrosine (NPY), a powerful inhibitor of glutamate release (Colmers et al., 1985). Taken together, it appears that the primary role of SOM-expressing interneurons is the regulation of dendritic inputs and signal integration. Indeed, the bistratified cell was recently shown to be a key controller of pyramidal cell output in vitro (Lovett-Barron et al., 2012, 2014).

The SOM-expressing bistratified and O-LM cell types in the CA1 area have nonoverlapping axonal arbors and are each selectively associated with one of the major glutamatergic inputs to pyramidal cells. Bistratified cells innervate the dendritic zones of pyramidal cells receiving input from the CA3 area (Buhl et al., 1994), whereas O-LM cells innervate the entorhinal input zone (McBain et al., 1994). Both cell types coexpress parvalbumin (PV), a calcium-binding protein that is also expressed by axoaxonic cells and one type of basket cell (Klausberger et al., 2003, 2004). Axoaxonic cells exclusively target axon initial segments and PV+ basket cells target proximal dendrites and somata; both release GABA but do not express SOM or NPY. The firing patterns of hippocampal interneurons are highly dependent on the network state, such as theta oscillations during movement or large-amplitude irregular network activity during sleep (Buzsáki, 2006; Ego-Stengel and Wilson, 2007; O'Keefe and Conway, 1978; Ranck, 1973). Drug-free behavior-dependent firing patterns of some identified cell types have been determined recently in freely moving rats (ivy cells, PV+ basket cells; Lapray et al., 2012) and in head-fixed mice (O-LM cells, PV+ basket cells; Varga et al., 2012), although for O-LM cells this did not include sleep. The firing patterns of identified bistratified cells in drug-free animals are unknown. We have recorded the firing of two distinct types of dendrite-targeting neuron in freely moving rats to test the hypothesis that differences in the axonal

terminations of SOM-expressing cells are associated with different firing patterns under natural awake behavior and sleep. This required the recording and labeling of SOM-expressing interneurons in freely moving rats using the juxtacellular labeling technique to identify the cells and enabled us to quantitatively dissect the firing dynamics of these cells and compare them to PV+ basket cells (Lapray et al., 2012), which target a different subcellular domain of pyramidal cells.

RESULTS

We have recorded the firing patterns of single interneurons using a glass electrode during periods of sleep, movement, and quiet wakefulness. Then, we either moved the electrode into a juxtacellular position or sometimes the cells spontaneously drifted close to the electrode, which made it possible to attempt labeling the cells with neurobiotin for identification of cell types. The labeled cells were assessed by immunofluorescence microscopy and tested for the presence of various molecules, including SOM and NPY. Nine identified interneurons (n = 9 rats, one cell each) were immunopositive for SOM, NPY, or both when tested by immunofluorescence microscopy and showed dendritic and axonal arborizations similar to previously described bistratified and O-LM cells (Buhl et al., 1994; McBain et al., 1994). The recording sites were distributed over an area of 1.7 × 1.4 mm along the rostrocaudal and mediolateral axes (Figure S1A available online).

Network Relationships of Bistratified and O-LM Cells

Somata of bistratified cells (n = 4/5 recovered) were located in the vicinity of pyramidal cell somata (Figures 1A and S1A and S1C), had mainly radially oriented dendritic trees (n = 3/5 recovered; see exception Figure S1C), and axon collaterals distributed in strata oriens and radiatum (n = 3/5 recovered). The axonal extent of a well-labeled cell was large (Figure 1A), reaching 2.4 mm mediolaterally and 1.7 mm rostrocaudally, confirming previous results obtained in vivo (Klausberger et al., 2004). Somata (n = 4/4 tested) were immunopositive for NPY (Figures 1B and S1E) and parvalbumin (PV), the latter also expressed in dendrites and axon (Figures 1C and S1D; Table 1). From the fifth interneuron (TV30d), we have only recovered some PV-immunopositive dendrites and the axon, which showed the characteristic bistratified distribution. These two features identified the cell as a bistratified cell. Somata were immunopositive for SOM (n = 3/4 tested; Figure 1B) (Klausberger et al., 2004), the metabotropic glutamate receptor type 1 alpha (mGluR1α; n = 1/2 tested), and one expressed the transcription factor Satb1 (n = 1/3 tested; Table 1). All three tested bistratified neurons had somatic and dendritic membranes enriched in tyrosine-protein kinase receptor ErbB4 (Figure 1D).

Cell bodies and horizontal spiny dendrites of recorded O-LM cells were in stratum oriens (n = 4/4 recovered; Figures 2A and S1A). The main axons (n = 3/4 recovered) originated from dendrites and projected into stratum lacunosum moleculare branching into a dense plexus (Figure 2A). From one O-LM cell (LK01ab), the axon was not recovered because of weak labeling. Somata (n = 4/4 tested) were immunopositive for SOM (Figure 2B), and dendritic and somatic membranes were enriched in mGluR1α (Figure 2D) and decorated by metabotropic glutamate receptor type 7a (mGluR7a)-immunopositive boutons (4/4 tested; Table 1). Three out of four tested O-LM cells were immunopositive for PV (Figure 2C), and three were immunopositive for the zinc finger protein transcription factor Fog-2 (Figure 2E). Two O-LM cells tested for extracellular leucine-rich repeat fibronectin-containing protein type 1 (Elfn1) were immunopositive (Figure 2F). None of the tested O-LM cells expressed calbindin or NPY (Table 1). The axon of one reconstructed O-LM cell (Figure 2A) had a mediolateral extent of 0.6 mm and a rostrocaudal extent of 1.1 mm.

Although the horizontal axonal extent of O-LM and bistratified cells are similar, their transmitter-releasing terminals are nearly completely separated in different layers, suggesting interactions with different glutamatergic inputs to pyramidal cells on segregated membrane domains. In order to compare their firing (Table 2), we segmented the spike time series according to different behavioral states based on quantitative parameters (Lapray et al., 2012). These were extracted from motion tracking and local field potential (LFP) measurements in the cortex and in the hippocampus (Figures 1E, 1F, 2G, and 2H). For O-LM cells, which are known to generate dendritic spikes (Martina et al., 2000), we cannot identify the origin of the spikes recorded.

Firing Rates and Interspike Interval Distributions of Bistratified, O-LM, and PV+ Basket Cells during Movement and Sleep

We have analyzed the activity of PV+ and neuropeptide-expressing bistratified and O-LM cells in relation to the reported activity of PV+ basket cells (Lapray et al., 2012), which do not express any known neuropeptide. In particular, our aim was to compare the spike timing of these three cell types and the influence of movement and sleep (Tables 3 and S3).

We have found that behavioral states have differential effects on the firing rates of bistratified (n = 5), O-LM (n = 4), and PV+ basket (n = 5; Lapray et al., 2012) cells (repeated-measures ANOVA, $F_{2,10} = 4.81$, $p = 0.0343$ for the interaction between the factors cell type and behavioral state; Figure 3A and Tables 2 and 3). During sleep, the mean firing rate of bistratified and PV+ basket cells was significantly higher by 16.9 and 19.2 Hz, respectively, than that of O-LM cells ($t(10) = 2.35$, $p = 0.0407$, for bistratified cells; $t(10) = 2.75$, $p = 0.0204$, for PV+ basket cells). As confirmed by their interspike interval (ISI) distributions (Figures 3B and S3), bistratified cells fired most frequently with high instantaneous frequency (IF) (5–12 Hz, 7.5%; 12–30 Hz, 11.9%; 30–100 Hz, 36.4%; 100–250 Hz, 35.1%), in contrast to O-LM cells, which showed IFs more often in the theta and beta ranges (5–12 Hz, 25.5%; 12–30 Hz, 25.3%; 30–100 Hz, 29.9%; 100–250 Hz, 8.8%).

During movement (Figures 3B and S3), the largest proportion of ISIs of both bistratified (42.2%) and O-LM (50.4%) cells corresponded to the gamma frequency range of firing (30–100 Hz). Bistratified cells (29.2%), but not O-LM cells (5.2%), frequently fired with ISIs shorter than 10 ms (IF > 100 Hz). Furthermore, the mean firing rate of bistratified and O-LM cells was higher during movement as compared to sleep, by 25.1% and 75.6%, respectively. In contrast, the mean firing rate of PV+ basket cells was lower by 22.9% during movement as compared to sleep.

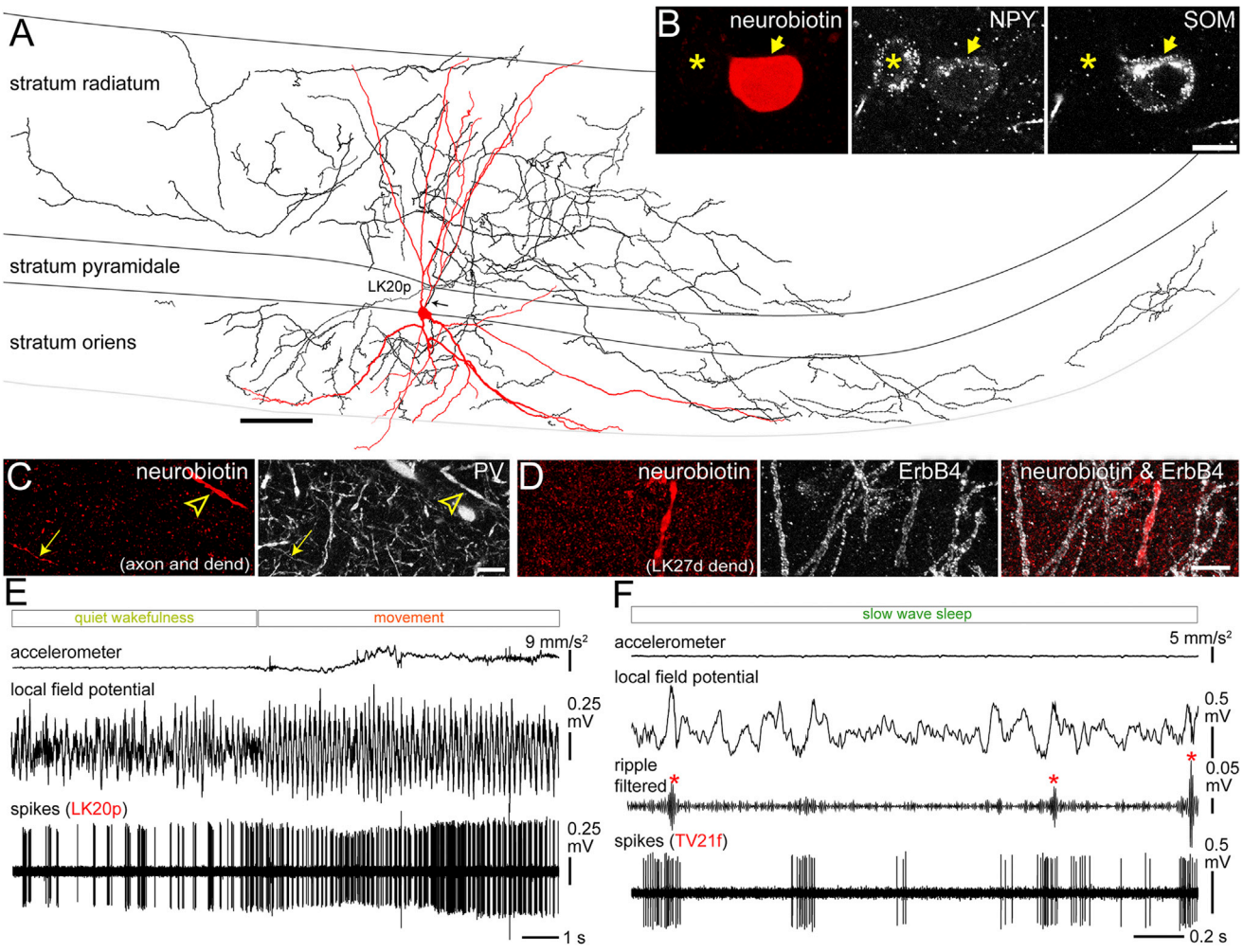

Figure 1. Behavior-Related Activity of Bistratified Cells

(A) Reconstruction of the soma, complete dendritic tree (red, n = 11 sections) and representative part of the axon (black, 3 of 24 70-μm-thick sections; axonal origin, arrow). Note the selective axonal arborization in strata oriens and radiatum, avoiding strata pyramidale and lacunosum moleculare. See also Figures S1 and S2.

(B) The soma (arrow) was immunopositive for NPY and SOM; a neighboring neuron (asterisk) was immunopositive only for NPY. Confocal single optical sections are shown (0.7 μm).

(C) The dendrite (arrowhead) and axon (arrow) were immunopositive for PV (maximum intensity projection, z stack, height 5.2 μm).

(D) The dendritic membrane of another tested bistratified cell (LK27d; Figure S1C) contained high levels of ErbB4 receptor (maximum intensity projection, z stack, height 15.0 μm). Scale bars, 100 μm in (A) and 10 μm (B)–(D).

(E) The bistratified cell increased its firing rate and changed to a more regular rhythmic pattern at a transition from quiet wakefulness to movement.

(F) Action potentials of another identified bistratified cell (TV21f) during slow-wave sleep. Note the SWR-related (asterisks) strong increases in the firing rate.

However, none of these apparent differences in firing rates within cell types between movement and sleep states were statistically significant (Table 3, repeated-measures ANOVA, post hoc pairwise comparisons, $p > 0.05$) due to the large cell-to-cell variability in the data. There was no difference in the mean firing rates between the three cell types during movement (Figure 3A) or during quiet wakefulness (Table S1).

Differential Involvement of Neuropeptide-Expressing Interneurons in Hippocampal Rhythmic Network Events

Rhythmic network activities emerge from the cooperative activity of specialized neuronal assemblies. We have segmented our LFP measurements into epochs of distinct oscillatory network states during different behaviors. We have detected theta oscillations (5–12 Hz; Figures 1E and 2G) during movement, sharp wave-associated ripples (SWRs; 130–230 Hz; Figures 1F, 2H, 5A, and 5B) during sleep and wakefulness, and low oscillatory periods (LOSC), which are often associated with state transitions (Lapray et al., 2012).

Bistratified (n = 5), O-LM (n = 4), and PV+ basket cells (n = 5; Lapray et al., 2012) fired with variable rates during theta oscillations, SWRs, and LOSC (repeated-measures ANOVA, $F_{4,21} = 22.27$, $p < 0.0001$ for the interaction between the factors cell type and network oscillatory state; Figure 4A and Tables 2

Table 1. Molecular Expression Profiles of Interneurons

	Immunohistochemical Test									
Cell	SOM	NPY	PV	CB	mGluR1a	mGluR7a	Elfn1/2	ErbB4	Fog-2	Satb1
Bistratified Cells										
K202j	+, s	+, s	+, s	nt	nt	nt	nt	nt	nt	nt
LK20p	+, s, d	+, s	+, s, d	−, d	−, s, d	nt	−, d	+, d	nt	+, s
LK27d	nc, s	+, s	+, s, d	nc, s	−, d	−, d	−, d	+, d	−, s	nc, s
TV21f	+, s	+, s	+, s	nc, s	+, s	nt	nt	nt	−, s	nc, s
TV30d	nc, a	nc, a	+, d	nt	nc, d	nt	nt	+, d	nt	nt
O-LM Cells										
LK01ab	+, s, d	−, s	+, d	nc, s	+, s, d	+, d	nt	nt	nc, s	nt
LK06ah	+, s, d	−, s	+, d	−, s, d	+, d	+, d	nt	nt	+, s	nt
LK13k	+, s	−, s	+, d	−, s, d	+, s, d	+, d	+, d	nt	+, s	nt
ZsB43d	+, s	−, s	−, s, d	−, s	+, d	+, d	+, d	nt	+, s	nt

+, immunopositive; −, no immunoreactivity detected in the cell, while other immunopositive cells were documented nearby; nc, not conclusive; nt, not tested; s, tested on soma; d, tested on dendrite; a, tested on axon.

and 3). During SWRs, the mean firing rates of bistratified and PV+ basket cells were higher by 94.6 Hz and 109.6 Hz, respectively, than that of O-LM cells ($t(21) = 8.75$, $p < 0.0001$, for bistratified cells; $t(21) = 10.14$, $p < 0.0001$, for PV+ basket cells). During SWRs, bistratified cells mostly fired above 100 Hz discharging with ISIs (67.0% of n = 1,486) of 4 to 10 ms (Figure 4C), whereas a much smaller proportion (33.8%) of O-LM cell ISIs (n = 86) corresponded to the >100 Hz frequency range.

During theta oscillations (Figure 4C), both bistratified and O-LM cells fired frequently (41.4% and 44.2%, respectively) within the gamma frequency range corresponding to ISIs of 10 to 33 ms. This resulted in a significant (73.3%) drop in the mean firing rate of bistratified cells ($t(21) = 7.45$, $p < 0.0001$), and a 55.7% increase in the firing rate of O-LM cells, as compared to firing rates during SWRs. The firing rates of both cell types were similar during LOSC (Figure 4C) to their respective rates during theta oscillations. No differences were found in mean firing rates between cell types during theta periods or during LOSC (Table 3; repeated-measures ANOVA, post hoc pairwise comparisons).

Changes in Spike Timing in Correlation with Network Oscillations

As a potential predictor of neuropeptide release, we have detected action potential burst patterns by bistratified (n = 5) and O-LM cells (n = 4), defined as at least three consecutive action potentials of ISIs, each ≤12 ms occurring during individual SWRs or individual theta oscillatory cycles. Bistratified cells fired such bursts (Figures 1E, 1F, and 5A) during 55.2% ± 4.7% of events (mean ± SEM) overall, significantly more (repeated-measures ANOVA, $F_{1,7} = 56.24$, $p = 0.0001$, for the factor cell type) than O-LM cells (Figures 2G, 2H, and 5B), which rarely emitted such bursts (2.7% ± 5.2%). This difference in the probability of bursting between bistratified and O-LM cells was independent of the network oscillatory event (see Tables 3 and S1). Similar differences were also revealed when testing for the occurrence of four consecutive action potentials, each ISI ≤ 12 ms.

Additionally, bistratified cells fired such bursts of three action potentials more frequently (2.8 ± 0.7 Hz; mean ± SEM) than O-LM cells (0.4 ± 0.7 Hz) during both movement and sleep (repeated-measures ANOVA, $F_{1,7} = 5.90$, $p = 0.0455$ for the factor cell type; Table 3 and Figure S2), suggesting that bistratified cells are more likely to release neuropeptides than O-LM cells during both movement and sleep. Thus, O-LM cells may be more selective in their release of SOM compared to bistratified cells during different behaviors.

Temporal Structure in Interneuron Firing during Theta and Ripple Oscillations

The spike timing of interneurons relative to the phase of ongoing theta cycles is informative of their postsynaptic effects on pyramidal cells, which fire with highest probability, on average, at the trough of theta oscillations (Buzsáki, 2006). We observed that the two SOM-expressing interneurons also fired strongly phase-coupled to the trough of theta oscillations recorded in strata pyramidale or oriens (Figure 4B and Table 2). The mean theta phases of bistratified (2.4° ± 19.4°, mean angle ± angular deviation; n = 5) and O-LM (341.6° ± 10.1°; n = 4) cells did not differ ($p = 0.1508$, permutation test [Tukker et al., 2007], difference 20.8°). The mean strength of phase coupling ($r = 0.33$, for both) was also similarly high ($p = 1$, permutation test, difference 0.0009) for the two cell types (Figure 4B and Table 2). Moreover, the pooled phase angle and coupling strength of bistratified and O-LM interneurons differed (permutation tests, mean phase difference, 64.4°; $p = 0.005$; mean strength of phase coupling difference 0.1685, $p = 0.0315$) from those reported for PV+ basket cells (n = 5; mean angle = 288.5° ± 44.4°, mean r = 0.15; Figure 4B; Lapray et al., 2012).

Next, we have investigated the firing dynamics of bistratified and O-LM cells during SWRs recorded either during sleep or wakefulness. Bistratified cells increased their firing rate strongly during SWRs (Figures 5A and 5D). In contrast, O-LM cells were mostly silent during SWRs (Figures 5B and 5E). Repeated-measures ANOVA ($F_{1,5} = 7.64$, $p = 0.0396$ for the interaction

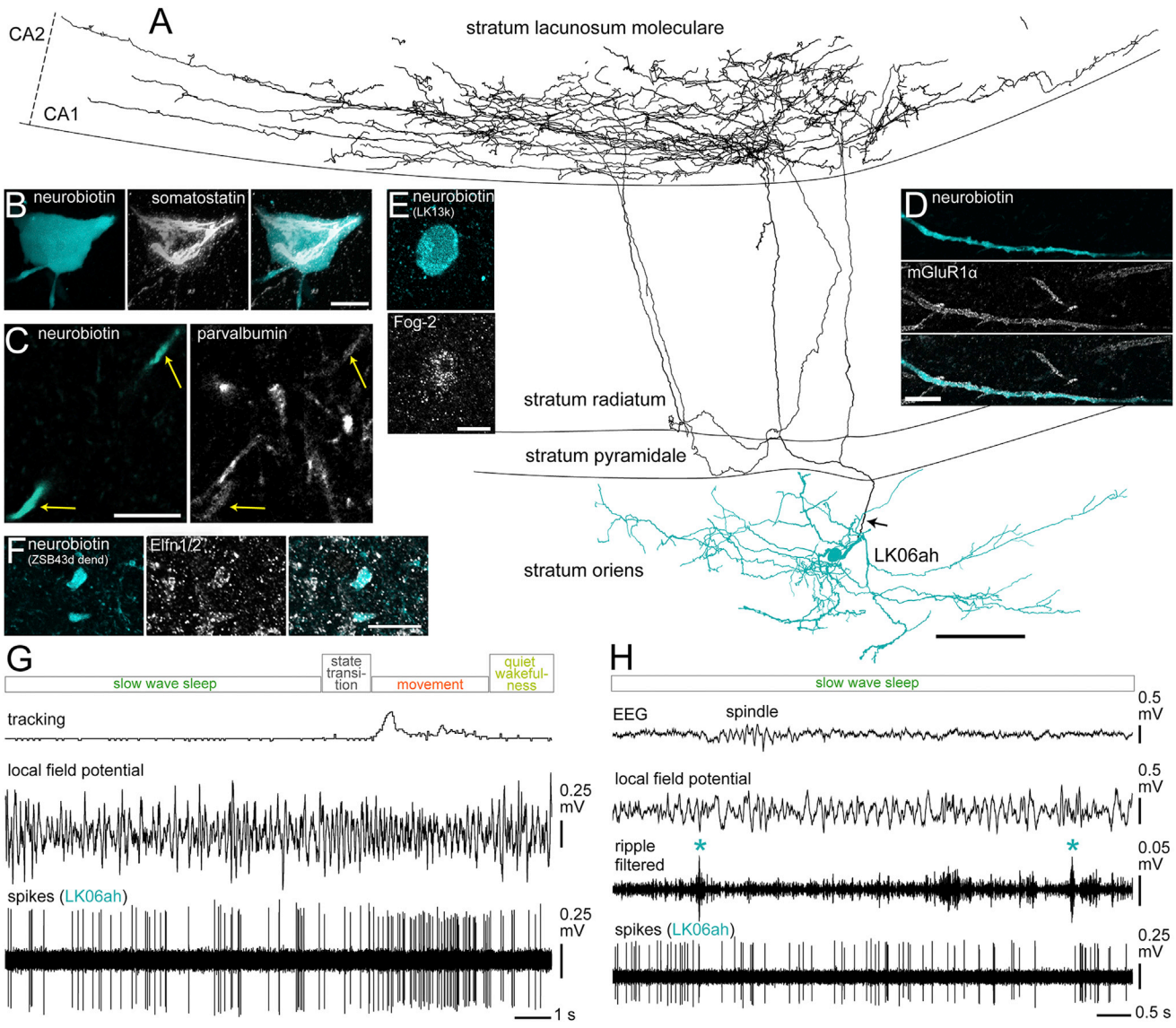

Figure 2. Activity of O-LM Cells Related to Behavior

(A) Reconstruction of the soma, complete dendritic tree (blue, n = 11 sections), and representative axon collaterals (black, 3 of 15 70-μm-thick sections; the main axon originated from a dendrite, arrow). Note the axonal plexus in stratum lacunosum moleculare and the lack of innervation of other layers. See also Figure S1.

(B) The soma was immunopositive for SOM (depth-cued projection z stack, height 28.7 μm).

(C) The dendrite (arrows) contained low levels of PV immunoreactivity (projection of two nonconsecutive optical sections, 0.7 μm each).

(D) The dendritic membrane was enriched in mGluR1a (maximum intensity projection, z stack, height 2.0 μm).

(E) Fog-2 was detected in the soma of another identified O-LM cell (single optical section, 0.7 μm).

(F) The dendrites of another recorded O-LM cell (ZsB43d) were immunopositive for Elfn1 (single optical section, 0.7 μm). Scale bars, 100 μm in (A) and 10 μm in (B)–(F).

(G and H) The rhythmic firing of the O-LM cell during movement (G) became irregular during slow-wave sleep (H). The cell did not appear to change its activity during SWRs (asterisks).

between the factors cell type and behavioral state) showed that bistratified cells (n = 5) fired significantly more spikes per SWR than O-LM cells (n = 4) (Figure 5C and Tables 2 and 3) during both sleep ($t(5) = 7.0$, $p = 0.0009$, mean difference 4.6) and wakefulness ($t(5) = 5.62$, $p = 0.0025$, mean difference 3.4). Moreover, O-LM, but not bistratified, cells had higher SWR-related spike counts during wakefulness compared to sleep ($t(5) = 3.62$, $p = 0.0152$, mean difference 1.3, for O-LM cells; $t(5) = -0.5$, $p = 0.6410$, mean difference 0.9, for bistratified cells; see also Tables 3 and S1).

The firing probability of bistratified cells was higher during SWRs than during periods of ±0.5 s before and after SWRs (Figure 5D). The firing rate during SWRs was two to six times higher (cumulative distribution functions, CDFs, $p < 0.05$ for n = 4 cells

Table 2. Firing Rates and Patterns of Interneurons

Cell	Mean Firing Rate					Mean Theta Phase of Firing	Mean Theta Vector Length of Firing[a]	Mean Number of Spikes per SWR		SWR-Activity Index[b]	
	Movement	Sleep	Quiet Wakefulness	Theta	SWRs	LOSC				Slow-Wave Sleep	Quiet Wakefulness
Bistratified Cells											
K202j	20.9 Hz	25.4 Hz	20.9 Hz	22.7 Hz	125.1 Hz	15.4 Hz	22.1° ± 71.4°	0.22	8.0	7.0	6.1	5.8
LK20p	42.6 Hz	NA	23.6 Hz	40.7 Hz	95.7 Hz	15.1 Hz	6.2° ± 59.9°	0.45	NA	4.0	NA	3.4
LK27d	37.9 Hz	19.5 Hz	32.2 Hz	34.9 Hz	65.2 Hz	17.0 Hz	350.9° ± 66.3°	0.33	3.0	3.0	2.3	3
TV21f	58.6 Hz	39.5 Hz	56.7 Hz	60.7 Hz	132.2 Hz	NA	21.3° ± 60.8°	0.44	8.5	6.0	2.1	2.3
TV30d	19.4 Hz	26.2 Hz	18.7 Hz	20.1 Hz	115.8 Hz	14.7 Hz	330.6° ± 68.9°	0.28	8.0	NA	5.2	NA
O-LM Cells												
LK01ab	17.5 Hz	11.0 Hz	15.6 Hz	17.0 Hz	13.3 Hz	16.1 Hz	356.2° ± 68.2°	0.29	0.0	1.0	1	1.3
LK06ah	18.5 Hz	9.2 Hz	15.3 Hz	16.9 Hz	16.8 Hz	15.9 Hz	333.1° ± 67.4°	0.31	1.0	1.5	1.6	1.6
LK13k	25.6 Hz	13.9 Hz	22.3 Hz	23.9 Hz	15.5 Hz	13.4 Hz	346.1° ± 59.4°	0.46	0.0	1.0	0.4	1.5
ZsB43d	21.9 Hz	13.4 Hz	16.0 Hz	18.0 Hz	3.1 Hz	15.7 Hz	331.3° ± 69.6°	0.26	0.0	0.0	0.1	0.3

[a]Theta modulation of firing [0,1], maximally correlated = 1; see Supplemental Experimental Procedures.
[b]Ratio of the mean firing rate during detected SWRs to the mean firing rate during the surrogate "SWR" population.

during sleep; $p < 0.05$ for n = 4 cells during wakefulness; Figures 5F and S4A and Table 2) than expected from the activity outside SWR time periods. In contrast, O-LM cells did not change their average firing probability during SWRs (Figure 5E). However, we have observed decreased or rarely increased firing rates during individual SWRs; and individual O-LM cells also slightly but significantly changed firing rates during SWRs in either direction (e.g., LK13k). During wakefulness, the firing rate during SWRs was significantly lower for one O-LM cell and higher for the other three cells than during sleep-SWRs (CDFs $p < 0.05$ for n = 4 cells; Figures 5G and S4B and Table 2). During sleep-SWRs, the mean rates were significantly decreased for two cells and increased for one cell (CDFs, $p < 0.05$ for n = 3 cells; Figures 5G and S4B and Table 2).

DISCUSSION

Our results demonstrate that SOM and GABA are released to distinct dendritic zones of CA1 pyramidal cells during sleep and awake states by bistratified and O-LM cells, differentially coordinating inputs from CA3 and entorhinal cortex, respectively. Both cell types activate postsynaptic $GABA_A$ receptors on pyramidal cell dendrites (Buhl et al., 1994; Maccaferri et al., 2000).

Modulatory Actions of Neuropeptides

Dendritic integration in pyramidal cell dendrites is nonlinear and involves voltage-dependent conductances (Losonczy and Magee, 2006; Spruston, 2008; Takahashi and Magee, 2009). The synergistic effects of SOM released by O-LM and bistratified cells and NPY released by bistratified cells are likely to regulate dendritic electrogenesis via pre- and postsynaptic receptors at a slower timescale than GABA. As peptide release is facilitated by high-frequency firing (van den Pol, 2012), such firing may predict peptidergic effects in physiological activity. The much higher frequency of burst firing by bistratified compared to O-LM cells, during movement and sleep, suggests that the CA3 input is under stronger peptidergic inhibition than the entorhinal input. Indeed, SOM (Tallent and Siggins, 1997) and NPY (Colmers et al., 1985) inhibit excitatory currents evoked by Schaffer collaterals (Boehm and Betz, 1997; Tallent and Siggins, 1997), and Y2 receptors are negatively coupled to N-type calcium channels on CA3 pyramidal cell terminals (Stanić et al., 2006). The calcium-dependent SOM release mechanism from O-LM cells probably requires fewer spikes and at lower frequencies compared to bistratified cells, as O-LM cells burst less frequently. Somatostatin receptors sst2R, sst3R, and sst4R are highly expressed by hippocampal and entorhinal glutamatergic neurons (Breder et al., 1992; Dournaud et al., 1996; Schreff et al., 2000; Schulz et al., 2000). In the entorhinal termination zone, sst2R immunoreactivity was described on terminals (Dournaud et al., 1996), possibly mediating the presynaptic inhibitory effect of O-LM cells. The sst3R knockout mice show impaired object-recognition memories (Einstein et al., 2010). Somatostatin can augment the voltage-sensitive noninactivating K+ M-current (I-M) (Moore et al., 1988) and increase a K+ leak current (Schweitzer et al., 1998) mediated by sst4R (Qiu et al., 2008). Bistratified cells are likely candidates for the activation of sst3R (Einstein et al.,

Table 3. Statistical Analyses

Repeated-measures ANOVA of mean firing rates of bistratified (BIC), O-LM and PV+ basket (PVBC) cells during movement and sleep

Type 3 test of fixed effects

Effect	df	F	p
cell type	2,11	3.22	0.08
behavioral state	1,10	1.55	0.24
interaction	2,10	4.81	0.03

Post hoc pairwise comparisons

	bistratified			O-LM			PV+ basket			movement vs sleep		
	df	t	p	df	t	p	df	t	p	df	t	P
BIC				10	2.35	0.04	10	-0.34	0.74	10	1.68	0.12
O-LM	10	-2.16	0.06				10	-2.75	0.02	10	2.07	0.06
PVBC	10	-1.84	0.10	10	0.43	0.68	movement		sleep	10	-1.85	0.09

Repeated-measures ANOVA of mean firing rates of bistratified (BIC), O-LM and PV+ basket (PVBC) cells during theta oscillations, SWRs and LOSC

Type 3 test of fixed effects

Effect	df	F	p
cell type	2,11	16.97	0.0004
oscillatory state	2,21	76.69	<0.0001
interaction	4,21	22.27	<0.0001

Post hoc pairwise comparisons

	Theta			SWRs			LOSC		
	df	t	p	df	t	p	df	t	p
BIC vs O-LM	21	1.56	0.13	21	8.75	<0.0001	21	0.15	0.88
BIC vs PVBC	21	1.48	0.15	21	-1.47	0.16	21	0.97	0.34
O-LM vs PVBC	21	-0.17	0.87	21	-10.14	<0.0001	21	0.82	0.42

	bistratified			O-LM			PV+ basket		
	df	t	p	df	t	p	df	t	p
Theta vs SWRs	21	-7.45	<0.0001	21	0.64	0.53	21	-10.60	<0.0001
Theta vs LOSC	21	1.85	0.08	21	0.34	0.73	21	1.50	0.15
SWRs vs LOSC	21	8.83	<0.0001	21	-0.29	0.77	21	12.1	<0.0001

Repeated-measures ANOVA of frequency of burst firing of bistratified (BIC) and O-LM cells during movement and sleep

Type 3 test of fixed effects

Effect	df	F	p
cell type	1,7	5.9	0.0455
behavioral state	1,6	0.66	0.4467
interaction	1,6	0.25	0.6327

Post hoc pairwise comparisons

	BIC vs O-LM		
	df	t	p
movement	6	2.39	0.05
sleep	6	1.79	0.12

	movement vs sleep		
	df	t	p
BIC	6	0.94	0.38
O-LM	6	0.22	0.84

Repeated-measures ANOVA of bursting probability of bistratified (BIC) and O-LM cells during theta cycles and SWRs

Type 3 test of fixed effects

Effect	df	F	p
cell type	1,7	56.24	0.0001
oscillatory state	1,7	1.79	0.2222
interaction	1,7	1.3	0.2921

Post hoc pairwise comparisons

	BIC vs O-LM		
	df	t	p
Theta	7	2.91	0.023
SWRs	7	4.86	0.002

	Theta vs SWRs		
	df	t	p
BIC	7	-1.86	0.11
O-LM	7	-0.13	0.90

Repeated-measures ANOVA of mean spike count of bistratified (BIC) and O-LM cells during awake- and sleep-SWRs

Type 3 test of fixed effects

Effect	df	F	p
cell type	1,7	42.49	0.0003
behavioral state	1,5	4.08	0.0994
interaction	1,5	7.64	0.0396

Post hoc pairwise comparisons

	BIC vs O-LM		
	df	t	p
awake	5	5.62	0.003
sleep	5	7.00	0.0009

	awake vs sleep		
	df	t	p
BIC	5	-0.5	0.64
O-LM	5	3.62	0.02

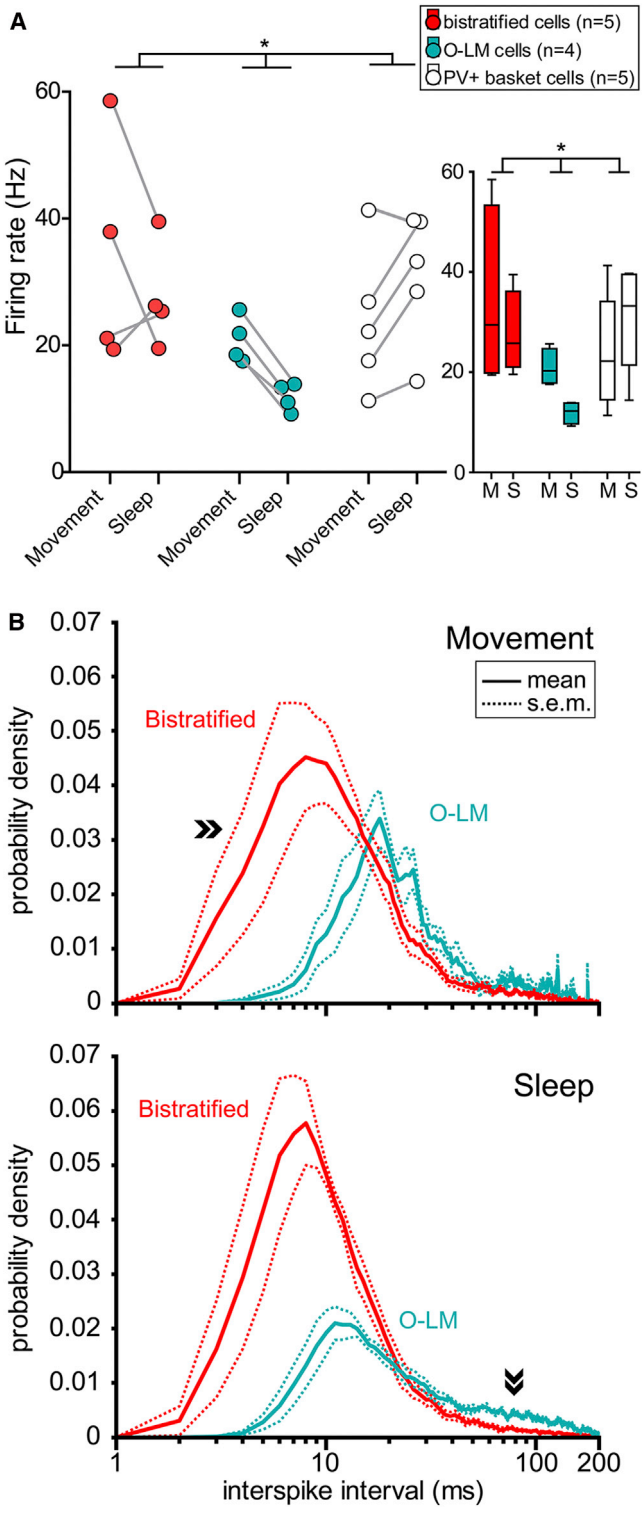

Figure 3. Firing Patterns of Bistratified, O-LM, and PV+ Basket Cells during Different Behavioral States

(A) Left: differences in firing rates between cell types changed with behavioral states ($p = 0.0343$ for the interaction; repeated-measures ANOVA). Right: box plot of cell-type- and behavioral state-dependent firing rates (horizontal line, median); M, movement; S, sleep.

(B) Interspike interval distributions (mean ± SEM) of bistratified (red) and O-LM (blue) cells during movement (top) and sleep (bottom) (see also Figure S3 and Table S3). Top: during movement, the largest proportion of interspike intervals of bistratified (42.2%) and O-LM (50.4%) cells were between 10 to 33 ms, corresponding to gamma frequency firing (30–100 Hz). Bistratified cells, but not O-LM cells, fired frequently (29.2%) with <10 ms intervals (>100 Hz, arrowheads). Bottom: during sleep, bistratified cells fired most frequently within fast frequency ranges (30–100 Hz and 100–250 Hz), discharging action potentials at intervals as short as 4 to 33 ms. In contrast, O-LM cells fired proportionally mostly at lower instantaneous frequencies with 10 to 200 ms intervals (arrowheads). Note that logarithmic timescales were limited to 200 ms.

2010) and sst4R (Schreff et al., 2000) due to their location on pyramidal cell dendrites. Activating the m1 muscarinic ACh receptor can inhibit the M-current (Dasari and Gulledge, 2011; Halliwell and Adams, 1982); hence, during theta oscillations when cholinergic tone is increased, levels of I-M activation are likely to be dominated by ACh-mediated suppression, and the augmentation by SOM may differ between active and inactive pyramidal cells due to the voltage sensitivity of the current. During SWRs, when SOM release from bistratified cells increases and cholinergic tone is low, augmentation of I-M may dominate and contribute synergistically with presynaptic Y2 receptor activation to the termination of SWRs. Presynaptic inhibitory effects by peptides (Breder et al., 1992; Schulz et al., 2000) and $GABA_B$ receptors are unlikely to block glutamate release; instead, they reduce release probability, thereby preserving presynaptic potency over periods of high presynaptic firing rates.

Interneuronal Control during Sharp Wave/Ripple and Theta Oscillations

During SWRs generated in CA3 (Buzsáki, 2006), single pyramidal cells rarely fire more than one to two action potentials, which individually would only have a weak effect on O-LM cells (Ali and Thomson, 1998) but stronger effects on bistratified cells (Ali et al., 1998). This is consistent with the strong activation of bistratified cells by simultaneous inputs from CA1 and CA3. The firing of bistratified cells (Klausberger et al., 2004) coupled to SWRs rarely dropped below 80 Hz, providing entrainment of the innervated small pyramidal cell dendrites in cooperation with PV+ basket cells that innervate the soma and proximal dendrites (Lapray et al., 2012; Varga et al., 2012). However, all O-LM cells were silent during at least some SWRs, and on average also decreased their firing, which indicates that some inhibitory input, activated during SWRs, contributes to their silencing. The O-LM cells are known to be innervated by vasoactive intestinal polypeptide-expressing, GABAergic interneuron-specific IS-III cells (Acsády et al., 1996; Chamberland et al., 2010) and also receive septal GABAergic innervation (Gulyás et al., 1990), which participate in their inhibition (Chamberland et al., 2010). Unfortunately, the activity patterns of neither of these GABAergic inputs are known in vivo. In any case, the withdrawal of GABA and SOM released by O-LM cells from the most distal dendrites in CA1 may enable the return input from the entorhinal cortex and a reverberation between CA1 and the entorhinal cortex during closely timed repeated ripples (Davidson et al., 2009). In the mouse, O-LM cells fired at higher rates in vitro during SWR-like

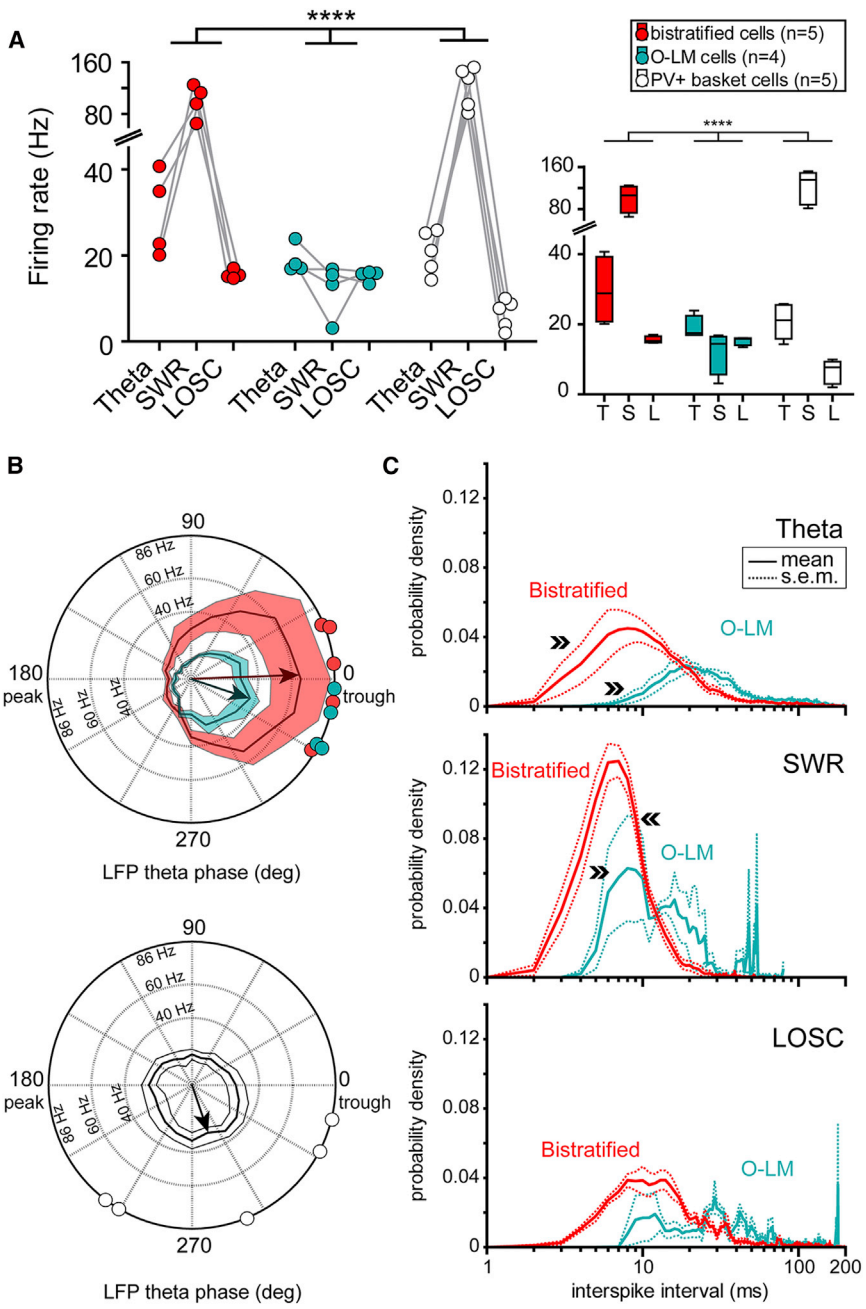

Figure 4. Bistratified, O-LM, and PV+ Basket Cell Activity during Network Oscillations

(A) Left: different mean firing rates during different network oscillatory states ($p < 0.0001$ for the interaction; repeated-measures ANOVA). Right: box plot of cell-type-specific and oscillatory state-dependent firing rates; T, theta oscillations; S, SWRs; L, LOSC.

(B) Preferred firing phases of bistratified, O-LM (top), and PV+ basket (bottom) cells during theta oscillations. Top: bistratified (red circles, individual cells; dark colored line, mean frequency; red area, SEM) and O-LM (blue circles and area) cells increased their firing probability around the trough of the theta cycle. The mean phase difference (20°) between the cell types (arrows) was not significant ($p = 0.1508$, permutation test). The two cell types were strongly phase modulated ($r = 0.33$, both). Bottom: in contrast, PV+ basket cells (white circles and area) fired at significantly earlier phases of the theta cycle ($p = 0.005$, permutation test) and showed weaker phase coupling ($r = 0.15$).

(C) Interspike interval distributions (mean ± SEM) of bistratified (red) and O-LM (blue) cells during theta oscillations (top), SWRs (middle), and LOSC (bottom) (see also Table S3). Top: during theta oscillations, bistratified cells fired spikes mostly (70.6%) at intervals between 4 to 33 ms corresponding to fast instantaneous firing frequencies (30–250 Hz, arrowheads); O-LM cells rarely fired within the 100–250 Hz range (4–10 ms, arrowheads, 3.3%). Middle: during SWRs, both cell types increased their instantaneous rates, although O-LM cells fired rarely. Bistratified cells fired mostly above 100 Hz (arrowheads, 67.0%), whereas a smaller proportion (33.8%) of O-LM cell interspike intervals were within 4 to 10 ms (100–250 Hz, arrowheads). Bottom: the distributions during LOSC were similar to those during theta oscillations. Note that logarithmic timescales were limited to 200 ms.

bursts in CA1 (Pangalos et al., 2013) and CA3 (Hájos et al., 2013) or during awake immobility in vivo (Varga et al., 2012). The difference between these reports and our results could be due to species differences, loss of some of the inhibitory circuits in vitro, and higher firing rates during SWRs in awake compared to sleep states. The O-LM cells reported here fired significantly more during awake-SWRs than during SWRs in sleep.

During theta oscillations, the pyramidal cell input to O-LM and bistratified cells may account for the firing of both cell types maximally around the theta trough, when pyramidal cells fire at highest probability in CA1. This was also predicted from tetrode recordings of pyramidal layer interneurons (Czurkó et al., 2011). However, the two cell types differ in that bistratified, but not O-LM, cells (Kim et al., 2012) receive input from CA3. Moreover, septal cholinergic input selectively activates O-LM cells via nicotinic acetylcholine receptors in arousal (Leão et al., 2012; Lovett-Barron et al., 2014). Both cell types are also likely to receive septal GABAergic innervation (Gulyás et al., 1990), which may include a population of PV-expressing medial septal neurons that discharge at the peak of theta in anesthetized rats (Borhegyi et al., 2004) and temporally lead hippocampal theta (Hangya et al., 2009). The sharp tuning and deep modulation by the theta rhythm of both cell types point to their collaborative role in the theta phase-dependent encoding and retrieval of spatial memories. An influential model of pyramidal cell synchronization (Hasselmo et al., 2002) posits that encoding of new sensory information is driven around the peak of the theta cycle,

corresponding to the entorhinal cortical input, and retrieval of stored contextual associations is strongest around the theta trough, which corresponds to the CA3 input. When an animal enters a place field, the place cell begins to fire around the theta peak, when both O-LM and bistratified cells are minimally active. This may enable encoding in place cell dendrites via long-term potentiation (LTP) at both CA3 and entorhinal synapses. Indeed, LTP is most easily evoked on the peak of theta oscillations (Hölscher et al., 1997). Coincident with a waning entorhinal input and an increasing CA3 input on the descending theta phase toward the trough, bistratified cell firing increases, enabling retrieval of stored associations undergoing modification from CA3 in place cell dendrites in strata radiatum and oriens of CA1. At the same phase, the increased O-LM cell activity probably plays a role in the removal of spurious entorhinal cortical input interfering with the recalled CA3 spatial context pattern (Hasselmo et al., 2002). Other GABAergic cell types that target the soma (Klausberger et al., 2005; Lapray et al., 2012; Varga et al., 2012) and axon initial segment (Viney et al., 2013) rather than dendrites provide different contributions to the temporal ordering and synchronization of pyramidal cell firing. The sharp theta phase tuning of SOM-expressing neurons indicates that there was little phase precession under our conditions. Unidentified interneurons show phase precession (Maurer et al., 2006), and some of them were suggested to be bistratified cells (Ego-Stengel and Wilson, 2007). The apparent lack of phase precession in our sample of interneurons may be due to the animals' slow movement (Ego-Stengel and Wilson, 2007).

Hypothesis for Differential Interneuron Action on Active and Silent Pyramidal Cells during Theta Oscillations

Pyramidal cells in CA1 can fire complex spikes, bursts of action potentials of decreasing amplitude riding on a slower dendritic calcium spike, often followed by a plateau potential (Epsztein et al., 2011; Kandel and Spencer, 1961; Pissadaki et al., 2010; Takahashi and Magee, 2009; Wong and Prince, 1978). Inhibition of SOM-expressing GABAergic neurons that innervate dendrites of neocortical pyramidal cells is necessary for such burst firing and calcium spikes evoked by sensory stimuli (Gentet et al., 2012). Further, in the hippocampus, inhibition of SOM-expressing interneurons in vivo promotes burst firing (Royer et al., 2012) and their activation in vitro greatly reduces the generation of calcium plateau potentials in pyramidal cells (Lovett-Barron et al., 2012). This suggests that dendrite-targeting O-LM and bistratified cells may reduce calcium spike generation of pyramidal cells in CA1. Extracellular recordings showed that the highest probability of burst firing in many, but not all, place cells occurs during entry at the periphery of the place field (Harris et al., 2001), probably coinciding with the peak of the theta cycle. In contrast, whole-cell recordings in vivo suggested that the highest probability of calcium and plateau potentials is in the middle or throughout the place field, coinciding with the highest firing rate (Epsztein et al., 2011). The extracellular theta LFP was not recorded in the above studies. The highest number of action potentials per theta cycle occurs at the trough in CA1 pyramidal cells (Mizuseki et al., 2009), usually corresponding to the middle of the place field. To reconcile the coincidence of the highest firing probability of active pyramidal cells, O-LM, and bistratified interneurons at the theta trough, we hypothesize a reduced effectiveness of the interneurons in inhibiting the calcium spike generation of active place cells, while inhibiting most silent pyramidal cells.

The increasing firing rate of active place cells was proposed to be partly due to the suppression of GABAergic input specifically to active cells, via increased postsynaptic calcium-dependent CB1 receptor-mediated retrograde signaling (Freund and Hájos, 2003). Interneurons expressing CB1 receptors fire on the ascending phase of theta cycles under anesthesia (Klausberger et al., 2005), which corresponds to the onset of place cell firing. Since SOM-expressing interneurons do not express CB1 receptors, GABA release may be suppressed at their terminals through other calcium-dependent retrograde signaling mechanisms, such as postsynaptic release of nitric oxide (NO) (Kaplan et al., 2013; McBain and Kauer, 2009), directly from the active place cells. Indeed, the calcium/calmodulin-dependent enzyme nNOS (Szabadits et al., 2007) and calcium-permeable NMDARs (Szabadits et al., 2011) are in the postsynaptic active zone of GABAergic synapses on pyramidal cells. Furthermore, NO-sensitive guanylyl cyclase (NOsGC) is present in GABAergic terminals (Szabadits et al., 2007), with the majority of PV-expressing and one-third of SOM-expressing interneurons expressing NOsGC subunits. Therefore, O-LM and bistratified cells may have the required molecular machinery for sensitivity to retrograde NO signaling. Activation of nNOS in pyramidal cell dendrites requires increases in local calcium concentrations via NMDARs and voltage-gated calcium channels in small-diameter dendrites innervated by the O-LM and bistratified cells. Therefore, active place cells may produce NO and selectively suppress GABA and SOM release presynaptically from connected O-LM and bistratified cells while simultaneously allowing the same interneurons to inhibit electrogenic processes in inactive pyramidal cells not participating in the current cell assembly. This selective reduction of inhibition to active cells may serve to increase the contrast between place cells and silent cells, facilitating dendritic calcium entry and synaptic plasticity in the active place cells. This scenario is consistent with the conversion of silent cells into place cells upon depolarization through an electrode (Lee et al., 2012).

Outlook

Our results obtained on the in vivo firing patterns of identified bistratified and O-LM cells, taken together with results on PV+ basket (Lapray et al., 2012; Varga et al., 2012) and axoaxonic cells (Viney et al., 2013) demonstrate that, on average, during each cycle of the theta oscillations, inhibition is redistributed from the axon initial segment through the soma to the progressively more distal dendrites of pyramidal cells, thus governing the repeated cycles of mnemonic processing such as memory encoding and retrieval in the hippocampal "chronocircuit" (Cutsuridis and Hasselmo, 2012; Dupret et al., 2013; Hasselmo et al., 2002). We hypothesize that the effect of these interneurons will be different on repeatedly firing versus silent pyramidal cells. Similarly, during SWRs, inhibition is redistributed by increased GABA release to the soma and CA3-innervated parts of the dendritic tree, while it is withdrawn from the axon

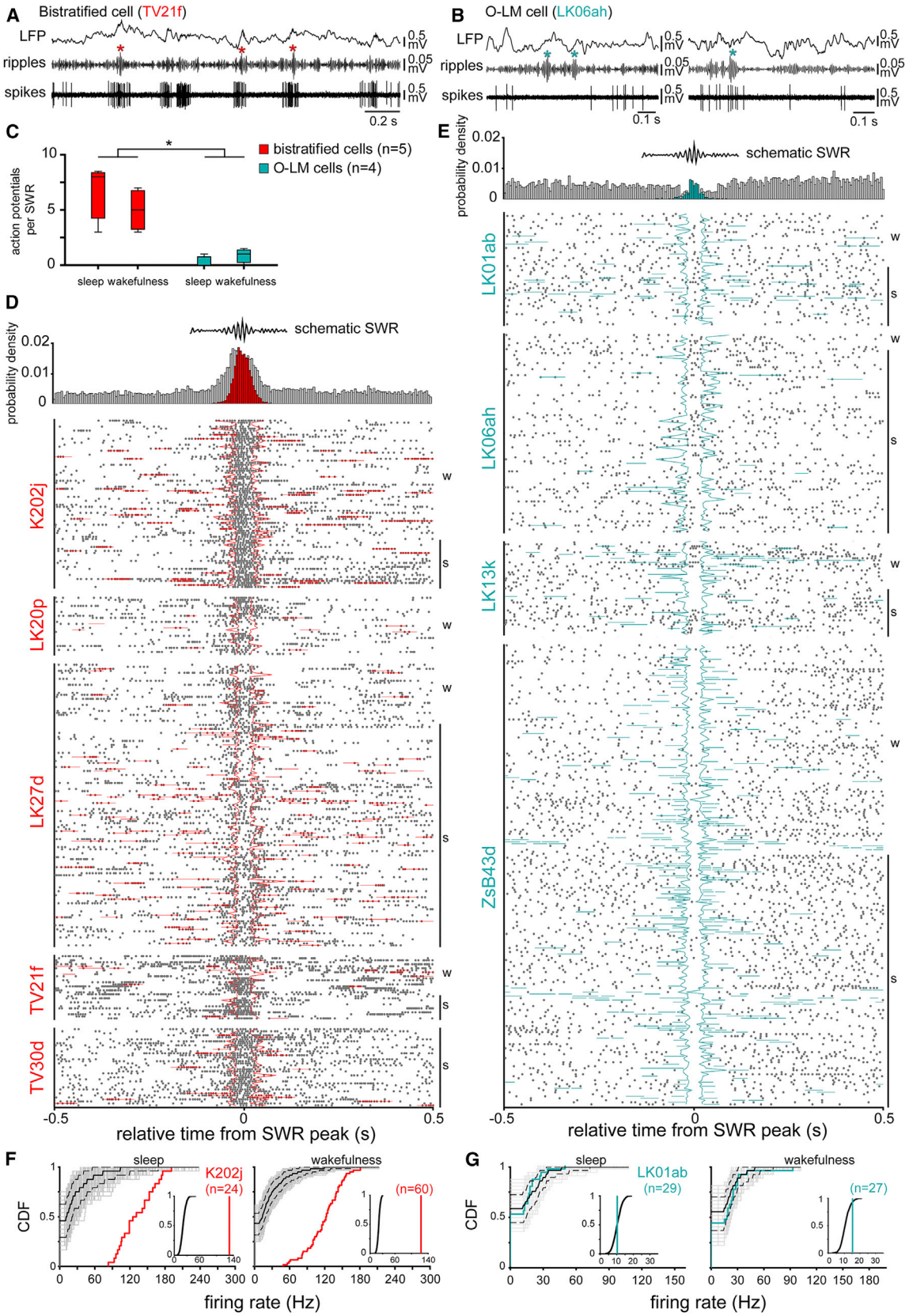

(legend on next page)

initial segment (Viney et al., 2013) and the entorhinal input zone of the dendrites, as shown here.

EXPERIMENTAL PROCEDURES

Experimental Subjects and Surgical Preparations

All procedures on animals were approved by the UK Home Office and by the Animal Care and Use Committees of the University of Oxford and of the Medical University, Vienna. Data reported are from nine male Sprague-Dawley rats (375–565 g; 2.8–5.3 months) recorded between 8 a.m. and 6 p.m. (see Supplemental Information). Implantations of the head-mounted recording setup, craniotomies, and duratomies were performed using analgesic and antibiotic treatments as reported in Lapray et al. (2012) (see Supplemental Information).

In Vivo Recordings and Juxtacellular Neurobiotin Labeling in Freely Moving Rats

Procedures were carried out as reported in Lapray et al. (2012). Rats were anesthetized briefly by isoflurane and connected to the recording setup. One hour after recovery, recordings commenced using a glass electrode (Figure S1B) filled with neurobiotin (1.5% or 3%, w/v, in 0.5 M NaCl). After recording and juxtacellularly labeling a cell, the rat was deeply anesthetized and perfusion fixed 1–3 hr later (see Supplemental Information).

Behavioral State Detection and Electrophysiological Data Analyses

Following the criteria defined in Lapray et al. (2012) (Figure 4), recording sessions have been segmented according to movement, sleep, and quiet wakefulness. We have detected and analyzed theta oscillatory epochs (5–12 Hz), SWRs (130–230 Hz), and LOSC using Spike2 and MATLAB (Wavelet Toolbox, v7.9-R2009b, MathWorks).

For a given cell type, we quantified the mean depth of theta modulation and the preferential mean theta phase of firing (circular mean ± circular SD) from individual cells using circular statistics and compared the preferred theta phase angles of different types of interneurons (see Supplemental Information).

Firing Rate Changes of Individual Interneurons during SWRs

We have developed an analysis in order to reveal the variability (e.g., cells being silent on some SWRs but firing with rates above average on others) in firing of single neurons during individual SWRs. Previous methods mostly used time-normalized averaging of firing during SWRs, or simply averaging aligned on SWR-peaks. Our approach captures quantitatively over the entire range of firing frequencies any differences in SWR-related spike rates compared to those expected from outside-SWR periods.

Method 1

Firing rates were calculated for the *n*-detected SWRs and their distribution displayed as a cumulative distribution function (CDF) (Figures 5F, 5G, S4A, and S4B). For some cells, these appeared to be Poisson-like. Next, a population of 1,000 × *n* surrogate time windows (surrogate "SWRs") was created as follows. (1) Periods of movement and of detected SWRs were excluded from the total recording time. The resulting sleep or rest states were considered as periods for SWRs to occur. (2) Random numbers were generated to mark time points within these periods when surrogate "SWRs" could occur. (3) Intervals of detected single SWR-lengths were placed, one by one, at the marked time points over the recorded spike train. Once a period was taken by a surrogate "SWR," it was not available for the subsequent ones. (4) After creating a surrogate for each detected SWR, individual firing rates were calculated and their distribution displayed as a CDF. These four steps were repeated 1,000 times, resulting in 1,000 CDFs (gray) representing the spiking of a given neuron outside detected SWRs. Next, the average of surrogate "SWRs" was computed as the median value (solid black line) at each frequency bin. The 95% confidence intervals (dashed black lines) were also plotted. Finally, for each neuron, the detected and derived firing rate distributions were compared using a two-sample Kolmogorov-Smirnov (KS) test. A probability of ≤ 0.05 indicates a significantly different firing rate distribution during detected SWRs from that calculated during outside SWR periods. A shift to the left or right of the measured firing rate distribution relative to the mean of the surrogate sets indicated a decreased or increased firing probability.

Method 2

The mean firing rate of a given neuron during the detected *n* SWRs was calculated by summing all spikes during the *n* SWRs and dividing this by the sum of durations of the *n* SWRs. A set of 1,000 × *n* surrogate "SWRs" was generated as above and the mean firing rate of each surrogate set was calculated, representing the spiking of a given neuron outside detected SWRs. In each sweep, spikes during *n* surrogate "SWRs" were counted and divided by the sum of time lengths of *n* SWRs. The CDF of the 1,000 surrogate mean firing rates was compared with the real mean firing rate during detected SWRs (insets in Figures 5F, 5G, S4A, and S4B). The crossing between the two lines shows the probability of the measured mean firing rate falling within or outside the population of surrogate rates obtained outside detected SWRs. If the probability was ≤ 0.05, then the mean firing rate of a given neuron during SWRs was considered significantly different from the firing rate during periods outside SWRs.

Statistical Comparison of Firing Rates and Spike Counts

Repeated-measures ANOVA analyses were performed in order to account for possible correlations between measurements from the same cell during different behavioral and network oscillatory states. In order to fit the model

Figure 5. Activity of Bistratified and O-LM Cells during SWRs

(A) Bistratified cells increased their firing rate strongly around and during SWRs (red asterisks). Top: LFP measured by an extracellular glass electrode in stratum pyramidale; middle: LFP band-pass filtered (130–230 Hz); bottom: action potentials of the recorded and labeled bistratified cell.

(B) O-LM cells were silent during the majority (left), but not all (right), SWRs (blue asterisks, both periods during sleep).

(C) Comparison of mean spike count per SWR of bistratified and O-LM cells recorded during sleep and wakefulness. The difference in spike counts between cell types depended on the behavioral state during which the SWRs occurred ($p = 0.0396$ for the interaction; repeated-measures ANOVA).

(D and E) Raster plots and average firing probability densities (top) of bistratified (D) and O-LM (E) cells relative to SWRs (w, wakefulness; s, sleep). Bistratified, but not O-LM cells, fired with higher probability during SWRs (colored bars in histogram) compared to the ±0.5 s (gray) surrounding the peak of SWR events. Overall, the firing probability of O-LM cells did not change during SWRs (blue bars in histogram); they decreased or rarely increased their firing probability. Raster plots were aligned to the peak SWR-power. Colored lines delineate the beginnings and ends of SWRs.

(F and G) Examples of SWR-related firing rates of bistratified (F) and O-LM (G) cells, during sleep and wakefulness. The distributions of measured firing rates per individual SWRs are displayed as cumulative distribution functions (CDFs). The distribution of bistratified cell firing rates (red) was significantly different from the median (black) of the surrogate sets ($p < 0.05$; two-sample KS test), and the right shift demonstrates an increase over the full range of firing rates. Surrogate sets of 1,000 firing rate-distributions are shown (gray; median, solid black line; 95% confidence intervals, broken lines). Insets: comparison of mean SWR-related firing rate (colored lines) with the distribution of surrogate mean SWR-related rates (black lines). The bistratified cell (red) was always strongly activated by SWRs ($p < 0.05$ for sleep; $p < 0.05$ for wakefulness, relative to the surrogate CDF). The measured distribution of the O-LM cell was also significantly different from the median (black) of the surrogate set ($p < 0.05$; two-sample KS test). The shift to the left or right of the measured CDF over part of the surrogate firing rate range indicates decreased or increased firing of the O-LM cell, respectively. Insets: during sleep, the mean firing rate of the O-LM cell (blue) was not different ($p = 0.137$, relative to the surrogate CDF) from the surrogate distribution (black). In contrast, during the awake condition, the measured mean firing rate of the O-LM cell was significantly increased during SWRs ($p = 0.035$, relative to the surrogate CDF). See also Figure S4.

consistently, the total number of cells was included in all cases, even when for a given cell either the behavioral states or the network oscillatory states were incomplete (LK20p, sleep data missing; TV21f LOSC data missing). We fitted a linear mixed effects model with restricted maximum likelihood estimation using the PROC MIXED procedure in SAS (v9.3)

$$Y_{ijk} = \mu + \alpha_i + \beta_j + (\alpha\beta)_{ij} + \varepsilon_{ijk},$$

where Y_{ijk} is the observed firing rate or SWR-related spike count of cell k of cell type i during within-factor behavioral/network oscillatory state, j; μ is the overall mean firing rate or overall mean spike count, α_i is the effect of cell type, i; β_j is the effect of within-factor behavioral/network oscillatory state, j; $(\alpha\beta)_{ij}$ is the interaction effect between cell-type and within-factor behavioral/network oscillatory state, and ε_{ijk} is random noise; all units are in Hz or counts. For simplicity, we defined the mixed model with compound symmetry as the correlation structure. This assumes similar variability between different cell types and equal correlation between different behavioral/network oscillatory states. For post hoc pairwise comparisons within the same model, differences of least-squares means of cell types were calculated for each level of within-factors, the behavioral/network oscillatory states, and vice versa, and the statistical significances were assessed. No adjustments were performed for multiple comparisons due to the low number of cells. For all statistical methods used in this paper, p values and confidence intervals were calculated according to $\alpha = 0.05$. Note that SWR-related spike counts (countX) were normalized using the following calculation: $\log_{10}(1 + \text{countX})$. When performed using median number of action potentials per SWR, the model did not result in significantly different conclusions from those given by mean spike counts, which we report.

We confirmed the predictions of the model using one-way ANOVA and Kruskal Wallis tests (Table S1).

Anatomical Analyses

One to three hours after cell labeling, cardiac perfusion with saline was followed by ~20 min fixation (4% paraformaldehyde w/v, 15% saturated picric acid v/v, and 0.05% glutaraldehyde w/v in 0.1 M phosphate buffer at pH ~7.2). All procedures, including transmitted light and fluorescence microscopic analyses were performed as reported in Lapray et al. (2012). Immunoreactivity in the recorded cells was assessed visually and compared to neighboring cells not labeled by neurobiotin. A positive signal in the recorded cell was accepted if the subcellular location (e.g., plasma membrane), pattern, and strength of the signal were similar to that in nonrecorded cells. None of the molecules that were located in the recorded cells are known to be expressed by pyramidal neurons, which provided a within-section negative control. Pyramidal cells express mGluR7a in a uniquely high level in their terminals innervating O-LM cells, a signal that is unmistakable. Two bistratified cells (LK20p, LK27d) and one O-LM cell (LK06ah) were selected for reconstruction (see Supplemental Information).

SUPPLEMENTAL INFORMATION

Supplemental Information includes Supplemental Experimental Procedures, four figures, and three tables and can be found with this article online at http://dx.doi.org/10.1016/j.neuron.2014.04.007.

ACKNOWLEDGMENTS

We thank K. Detzner, Sz. Biro, D. Kotzadimitriou, and Dr. J. Somogyi for advice and excellent technical support, Dr. B. Lasztoczi for help with analysis, and Dr. T. Szabadi and Sz. Biro for the reconstructions. One bistratified cell recoding was kindly provided by Dr. K. Hartwich. We thank Drs. Y. Dalezios and B. Hangya for advice on statistical analyses. We are grateful to Drs. Ray Guillery, D. Dupret, and B. Hangya for comments on an earlier version of the manuscript. We thank L. Papp (Neuronelektrod, Budapest, Hungary) for designing and manufacturing miniature reference electrode drives. Z.B. was supported by grant SCIC03 of the Vienna Science and Technology Fund.

Accepted: March 20, 2014
Published: May 1, 2014

REFERENCES

Acsády, L., Görcs, T.J., and Freund, T.F. (1996). Different populations of vasoactive intestinal polypeptide-immunoreactive interneurons are specialized to control pyramidal cells or interneurons in the hippocampus. Neuroscience *73*, 317–334.

Ali, A.B., and Thomson, A.M. (1998). Facilitating pyramid to horizontal oriens-alveus interneurone inputs: dual intracellular recordings in slices of rat hippocampus. J. Physiol. *507*, 185–199.

Ali, A.B., Deuchars, J., Pawelzik, H., and Thomson, A.M. (1998). CA1 pyramidal to basket and bistratified cell EPSPs: dual intracellular recordings in rat hippocampal slices. J. Physiol. *507*, 201–217.

Baude, A., Nusser, Z., Roberts, J.D.B., Mulvihill, E., McIlhinney, R.A., and Somogyi, P. (1993). The metabotropic glutamate receptor (mGluR1 α) is concentrated at perisynaptic membrane of neuronal subpopulations as detected by immunogold reaction. Neuron *11*, 771–787.

Boehm, S., and Betz, H. (1997). Somatostatin inhibits excitatory transmission at rat hippocampal synapses via presynaptic receptors. J. Neurosci. *17*, 4066–4075.

Borhegyi, Z., Varga, V., Szilágyi, N., Fabo, D., and Freund, T.F. (2004). Phase segregation of medial septal GABAergic neurons during hippocampal theta activity. J. Neurosci. *24*, 8470–8479.

Brazeau, P., Vale, W., Burgus, R., Ling, N., Butcher, M., Rivier, J., and Guillemin, R. (1973). Hypothalamic polypeptide that inhibits the secretion of immunoreactive pituitary growth hormone. Science *179*, 77–79.

Breder, C.D., Yamada, Y., Yasuda, K., Seino, S., Saper, C.B., and Bell, G.I. (1992). Differential expression of somatostatin receptor subtypes in brain. J. Neurosci. *12*, 3920–3934.

Buhl, E.H., Halasy, K., and Somogyi, P. (1994). Diverse sources of hippocampal unitary inhibitory postsynaptic potentials and the number of synaptic release sites. Nature *368*, 823–828.

Buzsáki, G. (2006). Rhythms of the Brain. (New York: Oxford University Press).

Chamberland, S., Salesse, C., Topolnik, D., and Topolnik, L. (2010). Synapse-specific inhibitory control of hippocampal feedback inhibitory circuit. Front. Cell Neurosci. *4*, 130, http://dx.doi.org/10.3389/fncel.2010.00130.

Chittajallu, R., Craig, M.T., McFarland, A., Yuan, X., Gerfen, S., Tricoire, L., Erkkila, B., Barron, S.C., Lopez, C.M., Liang, B.J., et al. (2013). Dual origins of functionally distinct O-LM interneurons revealed by differential 5-HT(3A)R expression. Nat. Neurosci. *16*, 1598–1607.

Colmers, W.F., Lukowiak, K., and Pittman, Q.J. (1985). Neuropeptide Y reduces orthodromically evoked population spike in rat hippocampal CA1 by a possibly presynaptic mechanism. Brain Res. *346*, 404–408.

Cutsuridis, V., and Hasselmo, M. (2012). GABAergic contributions to gating, timing, and phase precession of hippocampal neuronal activity during theta oscillations. Hippocampus *22*, 1597–1621.

Czurkó, A., Huxter, J., Li, Y., Hangya, B., and Muller, R.U. (2011). Theta phase classification of interneurons in the hippocampal formation of freely moving rats. J. Neurosci. *31*, 2938–2947.

Dasari, S., and Gulledge, A.T. (2011). M1 and M4 receptors modulate hippocampal pyramidal neurons. J. Neurophysiol. *105*, 779–792.

Davidson, T.J., Kloosterman, F., and Wilson, M.A. (2009). Hippocampal replay of extended experience. Neuron *63*, 497–507.

Dournaud, P., Gu, Y.Z., Schonbrunn, A., Mazella, J., Tannenbaum, G.S., and Beaudet, A. (1996). Localization of the somatostatin receptor SST2A in rat brain using a specific anti-peptide antibody. J. Neurosci. *16*, 4468–4478.

Dupret, D., O'Neill, J., and Csicsvari, J. (2013). Dynamic reconfiguration of hippocampal interneuron circuits during spatial learning. Neuron *78*, 166–180.

Ego-Stengel, V., and Wilson, M.A. (2007). Spatial selectivity and theta phase precession in CA1 interneurons. Hippocampus *17*, 161–174.

Einstein, E.B., Patterson, C.A., Hon, B.J., Regan, K.A., Reddi, J., Melnikoff, D.E., Mateer, M.J., Schulz, S., Johnson, B.N., and Tallent, M.K. (2010).

Somatostatin signaling in neuronal cilia is critical for object recognition memory. J. Neurosci. *30*, 4306–4314.

Epsztein, J., Brecht, M., and Lee, A.K. (2011). Intracellular determinants of hippocampal CA1 place and silent cell activity in a novel environment. Neuron *70*, 109–120.

Freund, T.F., and Hájos, N. (2003). Excitement reduces inhibition via endocannabinoids. Neuron *38*, 362–365.

Gentet, L.J., Kremer, Y., Taniguchi, H., Huang, Z.J., Staiger, J.F., and Petersen, C.C.H. (2012). Unique functional properties of somatostatin-expressing GABAergic neurons in mouse barrel cortex. Nat. Neurosci. *15*, 607–612.

Gulyás, A.I., Görcs, T.J., and Freund, T.F. (1990). Innervation of different peptide-containing neurons in the hippocampus by GABAergic septal afferents. Neuroscience *37*, 31–44.

Gulyás, A.I., Hájos, N., Katona, I., and Freund, T.F. (2003). Interneurons are the local targets of hippocampal inhibitory cells which project to the medial septum. Eur. J. Neurosci. *17*, 1861–1872.

Hájos, N., Karlócai, M.R., Németh, B., Ulbert, I., Monyer, H., Szabó, G., Erdélyi, F., Freund, T.F., and Gulyás, A.I. (2013). Input-output features of anatomically identified CA3 neurons during hippocampal sharp wave/ripple oscillation in vitro. J. Neurosci. *33*, 11677–11691.

Halliwell, J.V., and Adams, P.R. (1982). Voltage-clamp analysis of muscarinic excitation in hippocampal neurons. Brain Res. *250*, 71–92.

Hangya, B., Borhegyi, Z., Szilágyi, N., Freund, T.F., and Varga, V. (2009). GABAergic neurons of the medial septum lead the hippocampal network during theta activity. J. Neurosci. *29*, 8094–8102.

Harris, K.D., Hirase, H., Leinekugel, X., Henze, D.A., and Buzsáki, G. (2001). Temporal interaction between single spikes and complex spike bursts in hippocampal pyramidal cells. Neuron *32*, 141–149.

Hasselmo, M.E., Bodelón, C., and Wyble, B.P. (2002). A proposed function for hippocampal theta rhythm: separate phases of encoding and retrieval enhance reversal of prior learning. Neural Comput. *14*, 793–817.

Hölscher, C., Anwyl, R., and Rowan, M.J. (1997). Stimulation on the positive phase of hippocampal theta rhythm induces long-term potentiation that can Be depotentiated by stimulation on the negative phase in area CA1 in vivo. J. Neurosci. *17*, 6470–6477.

Jinno, S., Klausberger, T., Marton, L.F., Dalezios, Y., Roberts, J.D., Fuentealba, P., Bushong, E.A., Henze, D., Buzsáki, G., and Somogyi, P. (2007). Neuronal diversity in GABAergic long-range projections from the hippocampus. J. Neurosci. *27*, 8790–8804.

Kandel, E.R., and Spencer, W.A. (1961). Electrophysiology of hippocampal neurons. II. After-potentials and repetitive firing. J. Neurophysiol. *24*, 243–259.

Kaplan, J.S., Mohr, C., and Rossi, D.J. (2013). Opposite actions of alcohol on tonic GABA(A) receptor currents mediated by nNOS and PKC activity. Nat. Neurosci. *16*, 1783–1793.

Katona, I., Acsády, L., and Freund, T.F. (1999). Postsynaptic targets of somatostatin-immunoreactive interneurons in the rat hippocampus. Neuroscience *88*, 37–55.

Kim, J., Zhao, T., Petralia, R.S., Yu, Y., Peng, H., Myers, E., and Magee, J.C. (2012). mGRASP enables mapping mammalian synaptic connectivity with light microscopy. Nat. Methods *9*, 96–102.

Klausberger, T., Magill, P.J., Márton, L.F., Roberts, J.D.B., Cobden, P.M., Buzsáki, G., and Somogyi, P. (2003). Brain-state- and cell-type-specific firing of hippocampal interneurons in vivo. Nature *421*, 844–848.

Klausberger, T., Márton, L.F., Baude, A., Roberts, J.D.B., Magill, P.J., and Somogyi, P. (2004). Spike timing of dendrite-targeting bistratified cells during hippocampal network oscillations in vivo. Nat. Neurosci. *7*, 41–47.

Klausberger, T., Marton, L.F., O'Neill, J., Huck, J.H.J., Dalezios, Y., Fuentealba, P., Suen, W.Y., Papp, E., Kaneko, T., Watanabe, M., et al. (2005). Complementary roles of cholecystokinin- and parvalbumin-expressing GABAergic neurons in hippocampal network oscillations. J. Neurosci. *25*, 9782–9793.

Lapray, D., Lasztoczi, B., Lagler, M., Viney, T.J., Katona, L., Valenti, O., Hartwich, K., Borhegyi, Z., Somogyi, P., and Klausberger, T. (2012). Behavior-dependent specialization of identified hippocampal interneurons. Nat. Neurosci. *15*, 1265–1271.

Leão, R.N., Mikulovic, S., Leão, K.E., Munguba, H., Gezelius, H., Enjin, A., Patra, K., Eriksson, A., Loew, L.M., Tort, A.B.L., and Kullander, K. (2012). OLM interneurons differentially modulate CA3 and entorhinal inputs to hippocampal CA1 neurons. Nat. Neurosci. *15*, 1524–1530.

Lee, D., Lin, B.-J., and Lee, A.K. (2012). Hippocampal place fields emerge upon single-cell manipulation of excitability during behavior. Science *337*, 849–853.

Losonczy, A., and Magee, J.C. (2006). Integrative properties of radial oblique dendrites in hippocampal CA1 pyramidal neurons. Neuron *50*, 291–307.

Lovett-Barron, M., Turi, G.F., Kaifosh, P., Lee, P.H., Bolze, F., Sun, X.H., Nicoud, J.F., Zemelman, B.V., Sternson, S.M., and Losonczy, A. (2012). Regulation of neuronal input transformations by tunable dendritic inhibition. Nat. Neurosci. *15*, 423–430, S1–S3.

Lovett-Barron, M., Kaifosh, P., Kheirbek, M.A., Danielson, N., Zaremba, J.D., Reardon, T.R., Turi, G.F., Hen, R., Zemelman, B.V., and Losonczy, A. (2014). Dendritic inhibition in the hippocampus supports fear learning. Science *343*, 857–863.

Maccaferri, G., Roberts, J.D., Szucs, P., Cottingham, C.A., and Somogyi, P. (2000). Cell surface domain specific postsynaptic currents evoked by identified GABAergic neurones in rat hippocampus in vitro. J. Physiol. *524*, 91–116.

Martina, M., Vida, I., and Jonas, P. (2000). Distal initiation and active propagation of action potentials in interneuron dendrites. Science *287*, 295–300.

Maurer, A.P., Cowen, S.L., Burke, S.N., Barnes, C.A., and McNaughton, B.L. (2006). Phase precession in hippocampal interneurons showing strong functional coupling to individual pyramidal cells. J. Neurosci. *26*, 13485–13492.

McBain, C.J., and Kauer, J.A. (2009). Presynaptic plasticity: targeted control of inhibitory networks. Curr. Opin. Neurobiol. *19*, 254–262.

McBain, C.J., DiChiara, T.J., and Kauer, J.A. (1994). Activation of metabotropic glutamate receptors differentially affects two classes of hippocampal interneurons and potentiates excitatory synaptic transmission. J. Neurosci. *14*, 4433–4445.

Melzer, S., Michael, M., Caputi, A., Eliava, M., Fuchs, E.C., Whittington, M.A., and Monyer, H. (2012). Long-range-projecting GABAergic neurons modulate inhibition in hippocampus and entorhinal cortex. Science *335*, 1506–1510.

Mizuseki, K., Sirota, A., Pastalkova, E., and Buzsáki, G. (2009). Theta oscillations provide temporal windows for local circuit computation in the entorhinal-hippocampal loop. Neuron *64*, 267–280.

Moore, S.D., Madamba, S.G., Joëls, M., and Siggins, G.R. (1988). Somatostatin augments the M-current in hippocampal neurons. Science *239*, 278–280.

O'Keefe, J., and Conway, D.H. (1978). Hippocampal place units in the freely moving rat: why they fire where they fire. Exp. Brain Res. *31*, 573–590.

Pangalos, M., Donoso, J.R., Winterer, J., Zivkovic, A.R., Kempter, R., Maier, N., and Schmitz, D. (2013). Recruitment of oriens-lacunosum-moleculare interneurons during hippocampal ripples. Proc. Natl. Acad. Sci. USA *110*, 4398–4403.

Pissadaki, E.K., Sidiropoulou, K., Reczko, M., and Poirazi, P. (2010). Encoding of spatio-temporal input characteristics by a CA1 pyramidal neuron model. PLoS Comput. Biol. *6*, e1001038.

Qiu, C., Zeyda, T., Johnson, B., Hochgeschwender, U., de Lecea, L., and Tallent, M.K. (2008). Somatostatin receptor subtype 4 couples to the M-current to regulate seizures. J. Neurosci. *28*, 3567–3576.

Ranck, J.B., Jr. (1973). Studies on single neurons in dorsal hippocampal formation and septum in unrestrained rats. I. Behavioral correlates and firing repertoires. Exp. Neurol. *41*, 461–531.

Royer, S., Zemelman, B.V., Losonczy, A., Kim, J., Chance, F., Magee, J.C., and Buzsáki, G. (2012). Control of timing, rate and bursts of hippocampal place cells by dendritic and somatic inhibition. Nat. Neurosci. *15*, 769–775.

Schreff, M., Schulz, S., Händel, M., Keilhoff, G., Braun, H., Pereira, G., Klutzny, M., Schmidt, H., Wolf, G., and Höllt, V. (2000). Distribution, targeting, and internalization of the sst4 somatostatin receptor in rat brain. J. Neurosci. *20*, 3785–3797.

Schulz, S., Händel, M., Schreff, M., Schmidt, H., and Höllt, V. (2000). Localization of five somatostatin receptors in the rat central nervous system using subtype-specific antibodies. J. Physiol. Paris *94*, 259–264.

Schweitzer, P., Madamba, S.G., and Siggins, G.R. (1998). Somatostatin increases a voltage-insensitive K+ conductance in rat CA1 hippocampal neurons. J. Neurophysiol. *79*, 1230–1238.

Somogyi, P., Hodgson, A.J., Smith, A.D., Nunzi, M.G., Gorio, A., and Wu, J.Y. (1984). Different populations of GABAergic neurons in the visual cortex and hippocampus of cat contain somatostatin- or cholecystokinin-immunoreactive material. J. Neurosci. *4*, 2590–2603.

Spruston, N. (2008). Pyramidal neurons: dendritic structure and synaptic integration. Nat. Rev. Neurosci. *9*, 206–221.

Stanić, D., Brumovsky, P., Fetissov, S., Shuster, S., Herzog, H., and Hökfelt, T. (2006). Characterization of neuropeptide Y2 receptor protein expression in the mouse brain. I. Distribution in cell bodies and nerve terminals. J. Comp. Neurol. *499*, 357–390.

Szabadits, E., Cserép, C., Ludányi, A., Katona, I., Gracia-Llanes, J., Freund, T.F., and Nyíri, G. (2007). Hippocampal GABAergic synapses possess the molecular machinery for retrograde nitric oxide signaling. J. Neurosci. *27*, 8101–8111.

Szabadits, E., Cserép, C., Szőnyi, A., Fukazawa, Y., Shigemoto, R., Watanabe, M., Itohara, S., Freund, T.F., and Nyiri, G. (2011). NMDA receptors in hippocampal GABAergic synapses and their role in nitric oxide signaling. J. Neurosci. *31*, 5893–5904.

Takahashi, H., and Magee, J.C. (2009). Pathway interactions and synaptic plasticity in the dendritic tuft regions of CA1 pyramidal neurons. Neuron *62*, 102–111.

Tallent, M.K., and Siggins, G.R. (1997). Somatostatin depresses excitatory but not inhibitory neurotransmission in rat CA1 hippocampus. J. Neurophysiol. *78*, 3008–3018.

Tukker, J.J., Fuentealba, P., Hartwich, K., Somogyi, P., and Klausberger, T. (2007). Cell type-specific tuning of hippocampal interneuron firing during gamma oscillations in vivo. J. Neurosci. *27*, 8184–8189.

van den Pol, A.N. (2012). Neuropeptide transmission in brain circuits. Neuron *76*, 98–115.

Varga, C., Golshani, P., and Soltesz, I. (2012). Frequency-invariant temporal ordering of interneuronal discharges during hippocampal oscillations in awake mice. Proc. Natl. Acad. Sci. USA *109*, E2726–E2734.

Viney, T.J., Lasztoczi, B., Katona, L., Crump, M.G., Tukker, J.J., Klausberger, T., and Somogyi, P. (2013). Network state-dependent inhibition of identified hippocampal CA3 axo-axonic cells in vivo. Nat. Neurosci. *16*, 1802–1811.

Wong, R.K.S., and Prince, D.A. (1978). Participation of calcium spikes during intrinsic burst firing in hippocampal neurons. Brain Res. *159*, 385–390.

Neuron, Volume *82*

Supplemental Information

Sleep and Movement Differentiates Actions of Two Types of Somatostatin-Expressing GABAergic Interneuron in Rat Hippocampus

Linda Katona, Damien Lapray, Tim J. Viney, Abderrahim Oulhaj, Zsolt Borhegyi, Benjamin R. Micklem, Thomas Klausberger, and Peter Somogyi

1. Supplemental Figures

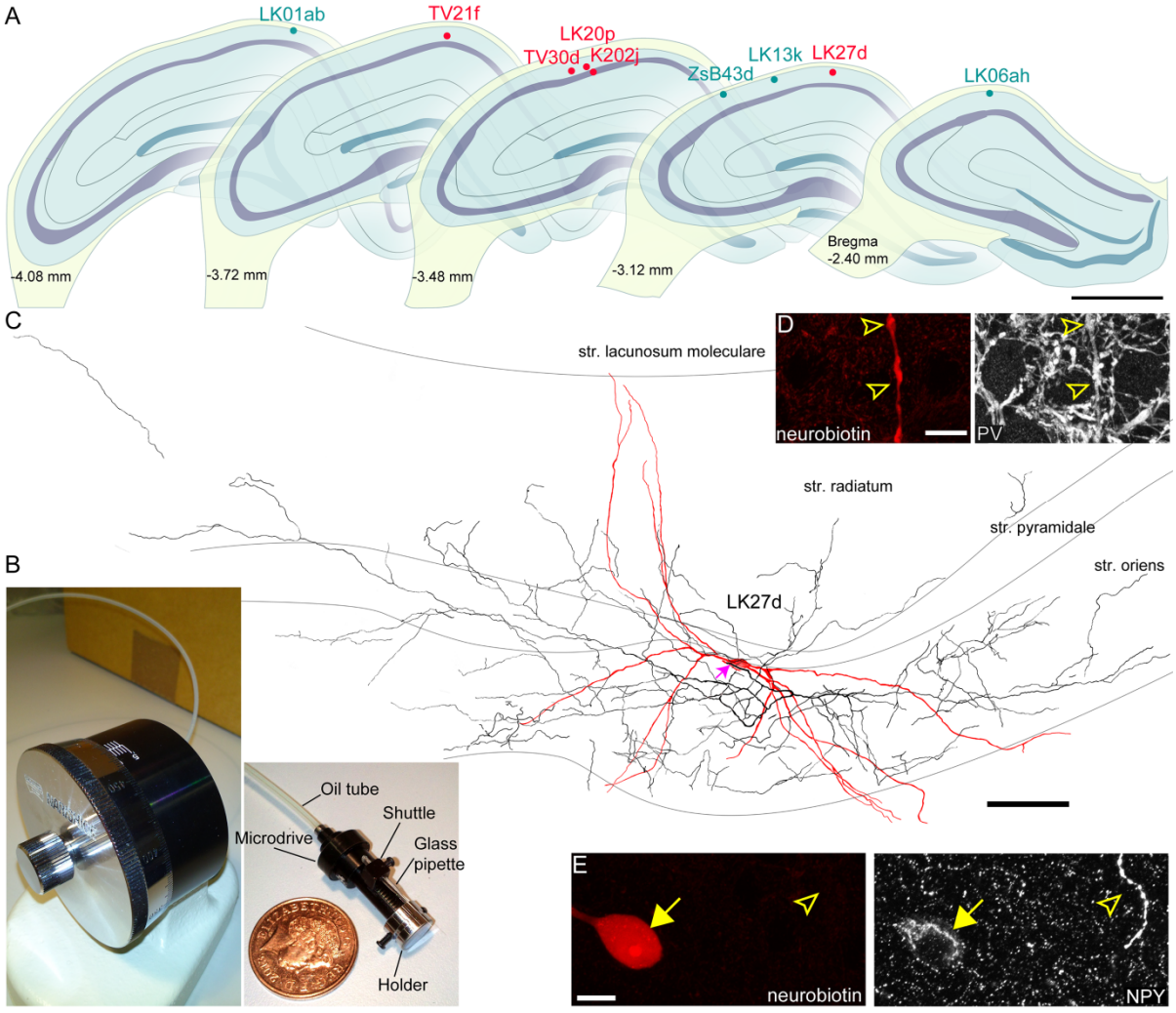

Figure S1. ***In vivo*** **extracellular recording and neurobiotin-labelling of single interneurons in freely moving rats and their positions in the hippocampus, related to Figures 1 and 2 and Experimental Procedures.** (A) Recording locations of labelled bistratified (red, n=5) and O-LM (blue, n=4) cells in CA1**.** Individual cell body locations in strata oriens and pyramidale are shown in schematic coronal sections from rostral to caudal direction, from left to right of the right hemisphere. Dark shaded bands show the pyramidal cell layer and the granule cell layer (blue) in the dentate gyrus. Scale bar, 1 mm. (B) Hydraulic (Narishige) microdrive *(right)* and manual manipulator *(left)*. *Right,* the metal holder is cemented to the rat's skull and

the microdrive is secured inside with screws. The shuttle holding the glass pipette is advanced by moving the manipulator connected via the oil tube. (C) Reconstruction of the soma, complete dendritic tree (red, n=9 ~70 μm thick sections) and representative part of the axon (black, 3 out of 20 70-μm-thick sections; axonal origin, magenta arrow) of a bistratified cell with a soma horizontally aligned with the pyramidal layer. Note the heavy axonal innervation of stratum oriens, but collaterals also entered stratum radiatum to a lower extent. (D) A tested dendrite (arrowheads) was immunopositive for PV (maximum intensity projection, z-stack, height 3.1 μm). (E) The cell body (arrow) and a neighbouring non-labelled axon (arrowhead) were immunopositive for NPY (maximum intensity projection, z-stack, height 3.9 μm). Scale bars, C 100 μm; D,E 10 μm.

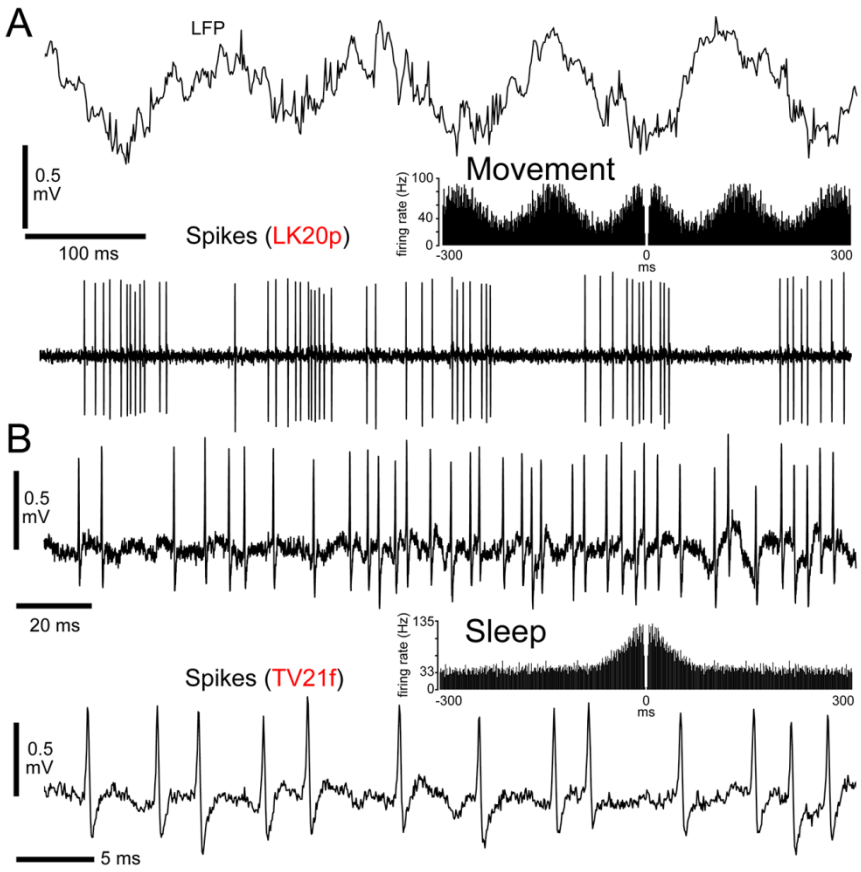

Figure S2. Firing patterns of bistratified cells during movement and sleep demonstrating short inter-spike intervals, related to Figures 1 and 3. (A) Spike train of a bistratified cell during movement. Note preferential timing of most spikes around the trough of the theta-oscillatory LFP (band-pass filtered 0.3-500 Hz). *Inset*, autocorrelogram of the interneuron. Note refractory period (1 ms time bins). (B) *Top*, spike train of a bistratified cell during sleep (band-pass filtered 0.8-5 kHz). *Bottom*, spike train at higher temporal resolution revealing uniform spike shapes. *Inset*, autocorrelogram of the interneuron. Note refractory period (1 ms time bins).

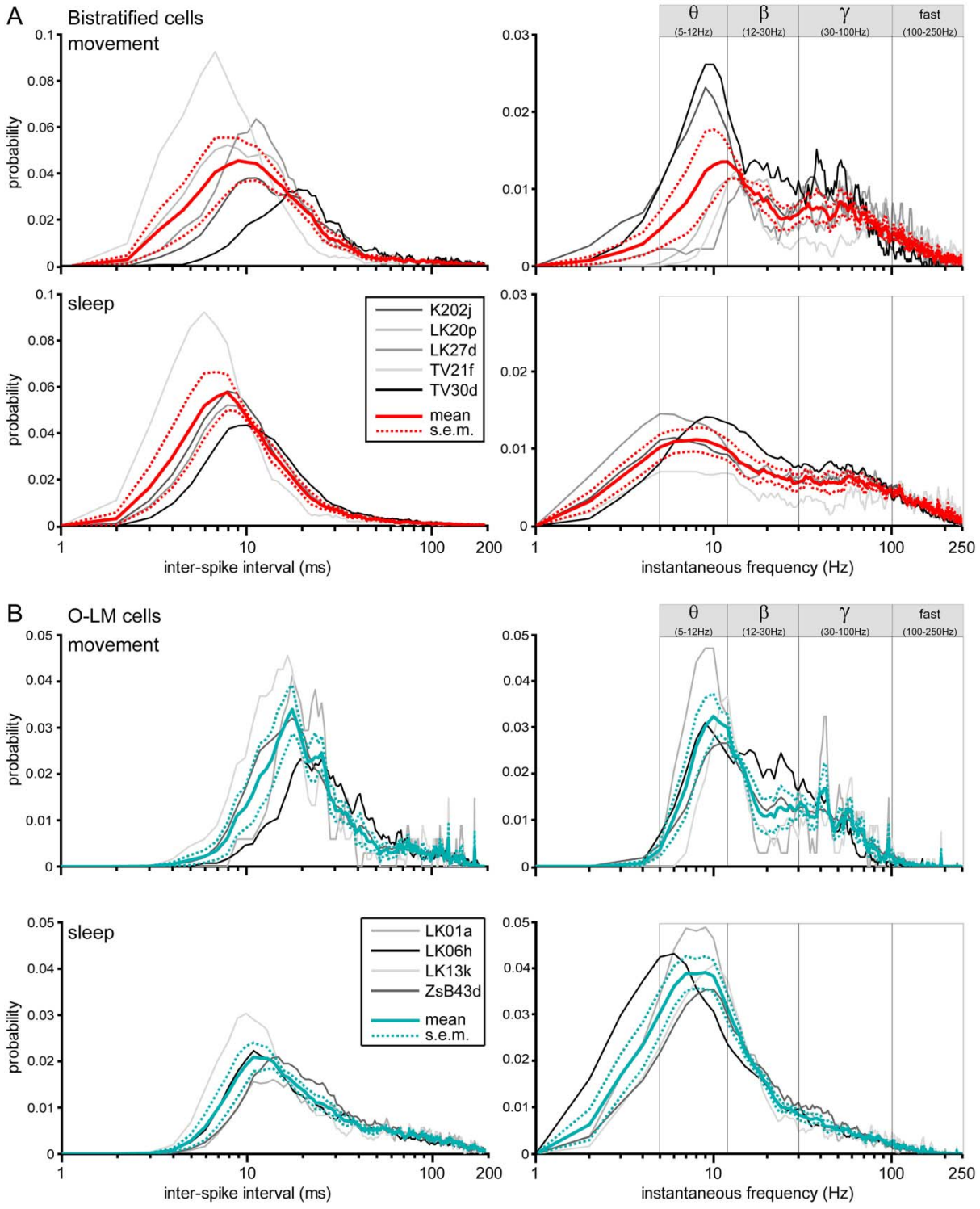

Figure S3. Individual inter-spike interval (ISI) and instantaneous frequency (IF) distributions of bistratified and O-LM cells, related to Figure 3. (A) *Left,* ISI distributions (mean ± s.e.m., solid and dashed lines) from all bistratified cells (individual cells, shades of grey; mean red) were calculated during sleep (*top*, n=4

cells) and movement (*bottom*, n=5 cells). Individual ISI distributions resembled each other more during sleep than during movement; TV21f had shorter ISIs than the other bistratified cells. *Right*, corresponding IF distributions across frequency ranges. (B) *Left*, ISI distributions (mean ± s.e.m., solid and dashed lines) from all O-LM cells (individual cells, shades of grey; mean blue) were calculated during sleep (*top*, n=4 cells) and movement (*bottom*, n=4 cells). Distributions were more similar during sleep than movement. Right, corresponding IF distributions. Note logarithmic time and frequency scales limited to 200 ms and 250 Hz, respectively.

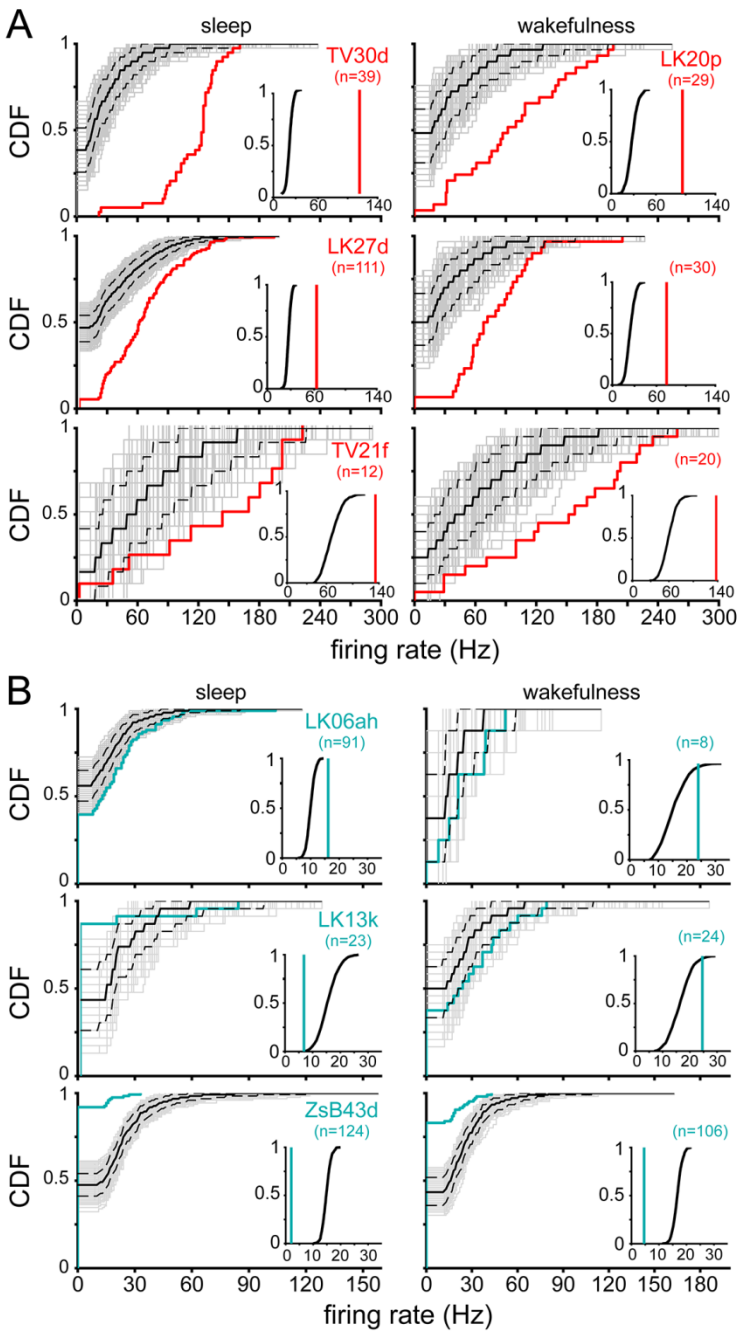

Figure S4. SWR-related firing rate distributions of bistratified and O-LM cells, during sleep and wakefulness, related to Figure 5. Bistratified cells (A) were activated by SWRs in all behavioural states (LK20p, no sleep period and TV30d no wakefulness recorded). The distribution of measured firing rates per individual SWRs are displayed as CDFs. For bistratified cells, the measured distributions (red) were significantly different from the medians (black) of the surrogate sets (2-sample KS-tests, n=4 cells in total, $p<0.05$ for all cells), and the right shift demonstrates an increase over the full range of firing rates. *Insets*, comparison of mean SWR-related firing rate (red lines), for each cell, with the distribution of surrogate mean rates (black lines). Bistratified cells (red) were strongly activated by SWRs, their measured mean rates were between 2 to 6 times higher than the means resulting from the surrogate distributions ($p<0.05$ for *sleep*; $p<0.05$ for *wakefulness*; relative to the CDFs for all four cells). O-LM cells (B)

changed their firing rates significantly during SWRs (2-sample KS-tests, n=3 cells in total, $p<0.05$, for all cells). The shift to the left or right of the measured CDFs (blue) relative to the median of the surrogate CDFs (grey) over the full or part of the surrogate firing rate range indicates decreased or increased firing of O-LM cells, respectively. Surrogate sets of 1000 firing rate-distributions (grey; median, solid black line; 95% confidence intervals, broken lines). *Insets*, comparison of mean SWR-related firing rate (blue lines), for each cell with the distribution of surrogate mean SWR-related rates (black lines). During *sleep*, the mean rates of LK13k and ZsB43d were decreased ($p=0.004$ for LK13k, $p=0$ for ZsB43d, probabilities given by CDFs) and the rate of LK06ah was increased ($p=0$, probability given by CDF). For cells LK06ah and LK13k in the *awake* condition, the measured rates were higher than those expected from the surrogate sets. *Insets*, comparison of mean SWR-related firing rates (blue lines) with the distribution of surrogate mean SWR-related rates (black lines). The rate of ZsB43d was decreased ($p=0$, relative to the CDF) and the rates of LK06ah and LK13k were increased ($p=0.01$ for LK06ah; $p=0.009$ for LK13k; probabilities given by CDFs) during SWRs. Note the differences in X axis scales between bistratified and O-LM cells in the insets.

Table S1. Statistical comparison of firing rates, bursting probability and spike counts of bistratified, O-LM and PV+ basket cells, related to Results.

			One-way ANOVA		Kruskal Wallis test	
Measure	**Comparison between**	**Condition**	**F**	**p**	**χ^2**	**p**
Firing rates	bistratified, O-LM and PV+ basket cells	movement	2.02 (2,11)	0.1788	2.5657	0.2772
		sleep	6.68 (2,10)	0.0144	7.9813	0.0185
		quiet wakefulness	2.28 (2,11)	0.1485	3.9057	0.1419
		theta oscillations	3.75 (2,11)	0.0572	4.7057	0.0951
		SWRs	23.73 (2,11)	0.0001	8.4629	0.0145
		LOSC	23.09 (2,10)	0.0002	8.6044	0.0135
Bursting probability	bistratified and O-LM cells	theta cycles	7.41 (1,7)	0.0297	6	0.0143
		SWRs	27.38 (1,7)	0.0012	6	0.0143
Mean number of spikes	bistratified and O-LM cells	sleep-SWRs	49.59 (1,6)	0.0004	5.3333	0.0209
		awake-SWRs	23.76 (1,6)	0.0028	5.3333	0.0209
	sleep-SWRs and awake-SWRs	bistratified cells	0.33 (1,6)	0.5864	0.3333	0.5637
		O-LM cells	1.36 (1,6)	0.2884	1.3333	0.2482

Table S2. Antibody information, related to Experimental Procedures.

Molecule	Host species	Internal ref No.	Dilution	Stock protein concentration (µg/ml)	Source	Source code
calbindin (CB)	rabbit	989	1:5000	antiserum	Swant, Bellinzona, Switzerland **(www.swant.com)**	CB-38 (lot 5.5)
tyrosine-protein kinase receptor (ErbB4)	mouse	1353	1:1000	200	Thermo Fisher Scientific, Kalamazoo, MI, USA **(www.labvision.com)**	MS-270-P, clone H4.77.16
extracellular leucine-rich repeat fibronectin containing protein-2 (Elfn 2)	rabbit	1432	1:500		Sigma-Aldrich, St. Louis, MO, USA **(www.sigma-aldrich.com)**	HPA000781
multizinc finger protein (Fog-2) M-247	rabbit	1369	1:200	200	Santa Cruz Biotechnology Inc., Santa Cruz,CA, USA **(www.scbt.com)**	sc-10755
metabotropic glutamate receptor-1 alpha subunit (mGluR1a)	goat	1266	1:750	1220	Prof. M. Watanabe, FRONTIER INSTITUTE Co. Ltd, Hokkaido, Japan	(Kind gift)
metabotropic glutamate receptor-1 alpha subunit (mGluR1a)	guinea pig	1267	1:500 1:1000 1:2000	660	Prof. M. Watanabe, FRONTIER INSTITUTE Co. Ltd, Hokkaido, Japan	(Kind gift)
metabotropic glutamate receptor-7 alpha subunit (mGluR7a)	rabbit	960	1:1000 1:2000	500	Prof. R. Shigemoto, Division of Cerebral Structure, Nat. Inst. Physiol. Sci, Okazaki, Japan	(Kind gift)
parvalbumin (PV)	goat	1258	1:1000 1:2000	antiserum	Swant, Bellinzona, Switzerland **(www.swant.com)**	PVG-214 (lot 3.6)
parvalbumin (PV)	guinea pig	1310	1:5000	antiserum	Synaptic Systems, Entwicklung und Produktion mbH, Goettingen, Germany **(www.sysy.com)**	195 004 (lot5)
parvalbumin (PV)	mouse	922	1:5000	antiserum	Swant, Bellinzona, Switzerland **(www.swant.com)**	235 (lot 10-11 F)
special AT-rich sequence-binding protein-1 (Satb1) N-14	goat	1394	1:200	200	Santa Cruz Biotechnology Inc., Santa Cruz,CA, USA **(www.scbt.com)**	sc-5989
special AT-rich sequence-binding protein-2 (Satb2) SATBA4B10	mouse	1341	1:100	100	Abcam, Cambridge, UK **(www.abcam.com)**	ab51502
special AT-rich sequence-binding protein-1 (Satb1) N-14	rabbit	1393	1:1000	1000	Abcam, Cambridge, UK **(www.abcam.com)**	ab70004
somatostatin (SM)	mouse	1276	1:200 1:400 1:500	140	GeneTex Inc., Irvine, CA, USA **(www.genetex.com)**	GTX71935 (clone SOM-018)
somatostatin (SM)	rat	815	1:500	1000	EMD Millipore Corporation, Billerica, MA, USA **(www.millipore.com)**	MAB354
neuropeptide Y (NPY)	rabbit	1011	1:5000	antiserum	ImmunoStar Inc.(DiaSorin), Hudson, WI, USA **(www.immunostar.com)**	22940 (lot 208001)

Molecule (repeated)	Host species	Epitope, amino acid residues	Antibody specificity information	Notes
calbindin (CB)	rabbit	polyclonal, recombinant rat calbindin D-28k	Knock out test in mouse: (Airaksinen et al., 1997); characterisation in rat hippocampus: (Sloviter, 1989).	
tyrosine-protein kinase receptor (ErbB4)	mouse	monoclonal, extracellular fragment, recombinant human c-erbB4/HER-4 oncoprotein	Generation, knock out tests, western blot band as expected: (Chen et al., 1996; Neddens et al., 2011; Vullhorst et al., 2009).	Cortical GABA circuit development controlled by ErbB4 signalling (Fazzari et al., 2010).
extracellular leucine-rich repeat fibronectin containing protein-2 (Elfn 2)	rabbit	polyclonal, affinity isolated, human ELFN2, recombinant protein epitope signature tag	Protein array and western blot tests: (Sylwestrak and Ghosh, 2012); developed and validated by the Human Protein Atlas project.	Labels interneurons via cross-reactivity with Elfn1.
multizinc finger protein (Fog-2) M-247	rabbit	polyclonal, epitope aa880-1126 mapping at the C-terminus of FOG-2 of mouse origin	Western blot by the company (Dale et al., 2007; Roche et al., 2008).	
metabotropic glutamate receptor-1 alpha subunit (mGluR1a)	goat		Personal communication with Prof. M. Watanabe.	In some interneurons it labels a reticular pattern instead of labelling the plasma membrane.
metabotropic glutamate receptor-1 alpha subunit (mGluR1a)	guinea pig	affinity purified	(Nakamura et al., 2004)	In some interneurons it labels a reticular pattern instead of labelling the plasma membrane.
metabotropic glutamate receptor-7 alpha subunit (mGluR7a)	rabbit	rat mGluR7 affinity purified, aa874-915	(Klausberger et al., 2005; Shigemoto et al., 1997; Shigemoto et al., 1996)	
parvalbumin (PV)	goat	polyclonal, rat muscle PV	Knock out tests in mouse: (Schwaller et al., 1999), Swant; western blot on rodent brain homogenate, single ~12 kDa band labelled (p. comm. E. Celio): (Constantinople et al., 2009).	
parvalbumin (PV)	guinea pig	polyclonal, recombinant full length rat PV	Western blot, abolished by pre-absorption with recombinant PV; knockout test in mouse:(Schwaller et al., 1999); same labelling with antibodies from: Synaptic Systems, rabbit 195 002, Swant, monoclonal 235; rat hippocampus: (Kosaka et al., 1987; Sloviter, 1989).	
parvalbumin (PV)	mouse	monoclonal, purified carp muscle PV	Knockout tests: in mouse (Schwaller et al., 1999); similar to other PV antibodies; characterization: (Celio et al., 1988).	
special AT-rich sequence-binding protein-1 (Satb1) N-14	goat	polyclonal, N-terminus, human SATB1	Knockout test in mouse: (Balamotis et al., 2012); mouse cortex: (Huang et al., 2011); same labelling as rabbit antibody ab70004.	Labels in addition SATB2-expressing nuclei in CA1 when used at 1:100 dilution. Weakly labels hilar neuron nuclei.
special AT-rich sequence-binding protein-2 (Satb2) SATBA4B10	mouse	monoclonal, recombinant fragment C-terminal, human SATB2.	Knockout tests in mouse: (Britanova et al., 2005; Britanova et al., 2008; Britanova et al., 2006; Dobreva et al., 2006); adult mouse brain: (Nielsen et al., 2010); same labelling as rabbit antibody ab34735 with additional signal for SATB1.	Labels pyramidal cells and a subpopulation of interneurons in CA1, consistent with the combination of specific SATB2 and SATB1 antibodies.
special AT-rich sequence-binding protein-1 (Satb1) N-14	rabbit	polyclonal, 18 aa near N-terminus, human SATB1	Knockout test in mouse: (Balamotis et al., 2012); mouse cortex: (Huang et al., 2011); no singal for knockout for a similar rabbit antibody; original rabbit antibody: (Dickinson et al., 1992); western blot in mouse, different band than SATB2 at P1; colocalization with NeuN, neuron specific.	Labels interneurons exclusively in hippocampus.
somatostatin (SM)	mouse	monoclonal, conjugated to protein carrier, human SOM	Rat antibody test: (Kubota et al., 2011); labelling pattern same as with rat antibody Chemicon MAB364; no signal in preabsorption test for rat antibody; mouse hippocampus using rat antibody: (Jinno and Kosaka, 2000).	Labels dendrites and axon stronger than other SOM antibodies.
somatostatin (SM)	rat	monoclonal, synthetic 1-14 cyclic SOM conjugated to bovine thyroglobulin using carbodiimide	Same labelling as other antibodies: (Kubota et al., 2011).	
neuropeptide Y (NPY)	rabbit	polyclonal, synthetic porcine NPY conjugated to methylated bovine serum albumin.	Antibody generation and characterization: (Allen et al., 1983); absorption-tested by manufacturer to 6 other peptides, no cross-reactivity observed; labelling as with other antibodies.	Strong immunoreactivity observed in subpopulations of hippocampal interneurons, no significant background.

Table S3. Point estimates of ISI distributions of bistratified and O-LM cells, related to Figure 3 and 4 and Supplemental Figure S3.

		Median ± interquartile range of ISI (ms)		
Cell type	**Cell**	**Movement**	**Sleep**	**Quiet wakefulness**
Bistratified cells	K202j	20.4 ± 37.3	13.2 ± 22.3	15.9 ± 31.1
	LK20p	12.6 ± 17.3	NA ± NA	12.9 ± 21.1
	LK27d	13.3 ± 14.3	15.0 ± 26.9	13.5 ± 16.8
	TV21f	7.7 ± 10.2	7.7 ± 10.9	7.3 ± 9.1
	TV30d	25.8 ± 43.4	17.4 ± 29.8	22.8 ± 42.5
O-LM cells	LK01ab	26.0 ± 66.4	65.6 ± 101.5	42.7 ± 66.3
	LK06ah	39.2 ± 44.6	54.8 ± 119.6	41.8 ± 60.2
	LK13k	22.5 ± 38.3	45.5 ± 87.8	26.2 ± 45.1
	ZsB43d	27.6 ± 43.7	44.4 ± 76.5	42.1 ± 57.5

Cell type	**Cell**	**Theta**	**SWRs**	**LOSC**
Bistratified cells	K202j	22.4 ± 36.3	6.4 ± 3.7	24.1 ± 73.2
	LK20p	13.2 ± 19.4	6.2 ± 4.3	20.9 ± 21.9
	LK27d	13.4 ± 15.4	8.9 ± 8.2	14.1 ± 19.8
	TV21f	7.6 ± 9.9	4.9 ± 2.9	NA ± NA
	TV30d	23.1 ± 46.7	6.7 ± 3.4	20.4 ± 46.4
O-LM cells	LK01ab	36.2 ± 66.2	15.0 ± 19.7	44.5 ± 54.5
	LK06ah	38.9 ± 54.3	14.9 ± 19.3	45.8 ± 53.0
	LK13k	23.3 ± 47.6	7.1 ± 4.1	30.0 ± 45.7
	ZsB43d	38.2 ± 53.8	20.1 ± 5.4	43.5 ± 60.1

2. Supplemental Experimental Procedures

Experimental subjects

Animals were housed in groups of 2–4 per cage in Oxford (8 rats; 19–21C°; 55% humidity; reverse light/dark cycle, lights on from 8pm–8am) or Vienna (1 rat; diurnal cycle, lights on from 6am–6pm). One to 7 days before the protocol started, rats were housed in a cage on their own with *ad libitum* access to food pellets and water. The rat in Vienna received chocolate chip rewards given during some recording sessions.

Microdrive, recording and reference electrodes

In short, we attached a cylindrical microdrive holder above the left parietal cortex using dental acrylic (Refobacin R, Biomet). A main connector was placed above the frontal part of the skull, supported by five stainless steel screws. EEG and reference-ground signals were fed into this head stage from one screw above the right prefrontal cortex (bregma -4 mm rostro-caudal, bregma +2 mm medio-lateral) and another above the cerebellum, respectively. Following recovery of a minimum of three days, the animal was anaesthetised, and after a craniotomy either a single wire electrode (50 μm tungsten, California Fine Wire; n=5 rats) fixed on the skull or movable by a miniature drive (Haiss et al., 2010) or a microdrive movable tetrode (n=4 rats) (Neuronelektrod Kft., Budapest, Hungary) was lowered into the right hippocampus or cortex. A layer of silicone (Kwik-Sil, World Precision Instruments) was used to protect the cortical surface between recordings.

In vivo behavioural recordings and juxtacellular neurobiotin-labelling in freely moving rats and data acquisition

Rats were anaesthetised briefly by isoflurane and a miniature preamplifier (NPI Electronic), two LED arrays and an accelerometer (Supertech Instruments; n=5

rats) were connected to the head stage. A glass electrode filled with neurobiotin (1.5 or 3%, wt/vol, in 0.5 M NaCl) was advanced using a hydraulic (Narishige, Figure S1B) or piezoelectric (Kleindiek Nanotechnik) (Lee et al., 2006) microdrive. Recordings commenced 1h after recovery from anaesthesia in a darkened room using a recording arena (40 $\times$ 40 cm floor; 27 cm walls or 50 $\times$ 50 cm floor, 27 cm walls in Oxford; 40 $\times$ 60cm floor, 30 cm walls in Vienna) to which the rats were naive on the first day. The rats were followed on two video cameras, one infra-red sensitive for behavioural analysis and another one for position tracking (software courtesy of Dr. K. Allen). Recordings were performed for 1–12 days (4.9 $\pm$ 3.1 days) after duratomy. After recording a cell, the pipette was advanced towards the neuron and juxtacellular labelling was attempted (Pinault, 1996). When deemed successful, the pipette was retracted slightly and the neuron was left to recover from the entrainment. The animal was deeply anaesthetised and perfusion fixed 1–3 h later. When stable neurons were not found sessions were finished by removal of the recording setup and by covering the cortical surface with silicone between consecutive days.

Signals were amplified 1000x (BF-48DGX and DPA-2FS, NPI Electronic) and digitised at 1 or 20 kHz (Power1401 A/D board, Cambridge Electronics Design). Measurements from the glass electrode were online band-pass filtered according to three different frequency ranges (0.3 Hz –10 kHz, wide-band; 0.3–500 Hz, LFP; 0.8–5 kHz, action potentials). Signals from the hippocampal/cortical electrodes were wide-band filtered. Elimination of 50 Hz noise without phase-shift was provided by Hum Bugs (Quest Scientific Instruments). Accelerometer measurements were digitised at 1 or 20 kHz. Acquisition of all signals, except tracking, went in parallel using Spike2 software (v7.01, Cambridge Electronics Design).

Electrophysiological data analyses

For each interneuron, we computed the theta phases of the recorded spikes. We determined whether the cell was theta modulated using Rayleigh's method (Zar, 1999) and if the theta phases resulted in a non-uniform distribution around the theta cycle. Using normalised vector addition, we calculated the cell's mean phase angle and the depth of the cell's theta modulation. Data was averaged across individual cells of the same type. For the quantitative comparison of distinct cell types we used two-sample permutation tests (Good, 2000).

Recorded spike trains were segmented according to behavioural and oscillatory network states and analysed one by one. For each interneuron, the periods between two consecutive action potentials (ISI) have been measured and their distributions analysed. The ISI distributions of individual cells of a given type were averaged and the resulting mean $\pm$ s.e.m. was considered as the representative ISI distribution for the cell type during a given state. Additionally, we calculated point estimates (median $\pm$ interquartile range) for the individual ISI distributions per cell and per state (Table S3).

Neuronal 3D reconstructions

Neurons were digitally reconstructed in 3D from resin-embedded, osmium-treated sections reacted for HRP using Neurolucida (MBF Bioscience), a Nikon Eclipse 80i transmitted light microscope and Lucivid microdisplay (MBF Bioscience) in continuous mode using a VC Plan Apo 100x/1.4 oil immersion objective.

Antibody information

Secondary antibodies conjugated to Alexa488 and Alexa405 fluorophores were purchased from Invitrogen. Secondary antibodies conjugated to Cy3, Cy5, DyLight405, DyLight488, DyLight594 and DyLight649 fluorophores were purchased from Stratech.

3. Supplemental References

Airaksinen, M.S., Eilers, J., Garaschuk, O., Thoenen, H., Konnerth, A., and Meyer, M. (1997). Ataxia and altered dendritic calcium signaling in mice carrying a targeted null mutation of the calbindin D28k gene. Proc. Natl. Acad. Sci. USA 94, 1488-1493.

Allen, Y.S., Adrian, T.E., Allen, J.M., Tatemoto, K., Crow, T.J., Bloom, S.R., and Polak, J.M. (1983). Neuropeptide Y distribution in the rat brain. Science 221, 877-879.

Balamotis, M.A., Tamberg, N., Woo, Y.J., Li, J., Davy, B., Kohwi-Shigematsu, T., and Kohwi, Y. (2012). Satb1 ablation alters temporal expression of immediate early genes and reduces dendritic spine density during postnatal brain development. Mol. Cell Biol. 32, 333-347.

Britanova, O., Akopov, S., Lukyanov, S., Gruss, P., and Tarabykin, V. (2005). Novel transcription factor Satb2 interacts with matrix attachment region DNA elements in a tissue-specific manner and demonstrates cell-type-dependent expression in the developing mouse CNS. Eur. J. Neurosci. 21, 658-668.

Britanova, O., de Juan Romero, C., Cheung, A., Kwan, K.Y., Schwark, M., Gyorgy, A., Vogel, T., Akopov, S., Mitkovski, M., Agoston, D*., et al.* (2008). Satb2 is a postmitotic determinant for upper-layer neuron specification in the neocortex. Neuron 57, 378-392.

Britanova, O., Depew, M.J., Schwark, M., Thomas, B.L., Miletich, I., Sharpe, P., and Tarabykin, V. (2006). Satb2 haploinsufficiency phenocopies 2q32-q33 deletions, whereas loss suggests a fundamental role in the coordination of jaw development. Am. J. Hum. Genet. 79, 668-678.

Celio, M.R., Baier, W., Schärer, L., De Viragh, P.A., and Gerday, C. (1988). Monoclonal antibodies directed against the calcium binding protein parvalbumin. Cell Calcium 9, 81-86.

Chen, X., Levkowitz, G., Tzahar, E., Karunagaran, D., Lavi, S., Ben-Baruch, N., Leitner, O., Ratzkin, B.J., Bacus, S.S., and Yarden, Y. (1996). An immunological approach reveals biological differences between the two NDF/Heregulin receptors, ErbB-3 and ErbB-4. J. Biol. Chem. 271, 7620-7629.

Constantinople, C.M., Disney, A.A., Maffie, J., Rudy, B., and Hawken, M.J. (2009). Quantitative analysis of neurons with Kv3 potassium channel subunits, Kv3.1b and Kv3.2, in macaque primary visual cortex. J. Comp. Neurol. 516, 291-311.

Dale, R.M., Remo, B.F., and Svensson, E.C. (2007). An alternative transcript of the FOG-2 gene encodes a FOG-2 isoform lacking the FOG repression motif. Biochem. Biophys. Res. Commun. 357, 683-687.

Dickinson, L.A., Joh, T., Kohwi, Y., and Kohwi-Shigematsu, T. (1992). A tissue-specific MARSAR DNA-binding protein with unusual binding site recognition. Cell 70, 631-645.

Dobreva, G., Chahrour, M., Dautzenberg, M., Chirivella, L., Kanzler, B., Fariñas, I., Karsenty, G., and Grosschedl, R. (2006). SATB2 is a multifunctional determinant of craniofacial patterning and osteoblast differentiation. Cell 125, 971-986.

Fazzari, P., Paternain, A.V., Valiente, M., Pla, R., Lujan, R., Lloyd, K., Lerma, J., Marin, O., and Rico, B. (2010). Control of cortical GABA circuitry development by Nrg1 and ErbB4 signalling. Nature 464, 1376-1380.

Good, P. (2000). Permutation tests : a practical guide to resampling methods for testing hypotheses (New York: Springer).

Haiss, F., Butovas, S., and Schwarz, C. (2010). A miniaturized chronic microelectrode drive for awake behaving head restrained mice and rats. J. Neurosci. Methods 187, 67-72.

Huang, Y., Zhang, L., Song, N.-N., Hu, Z.-L., Chen, J.-Y., and Ding, Y.-Q. (2011). Distribution of Satb1 in the central nervous system of adult mice. Neurosci. Res. 71, 12-21.

Jinno, S., and Kosaka, T. (2000). Colocalization of parvalbumin and somatostatin-like immunoreactivity in the mouse hippocampus: Quantitative analysis with optical disector. J. Comp. Neurol. 428, 377-388.

Klausberger, T., Marton, L.F., O'Neill, J., Huck, J.H.J., Dalezios, Y., Fuentealba, P., Suen, W.Y., Papp, E., Kaneko, T., Watanabe, M.*, et al.* (2005). Complementary roles of cholecystokinin- and parvalbumin-expressing GABAergic neurons in hippocampal network oscillations. J. Neurosci. 25, 9782-9793.

Kosaka, T., Katsumaru, H., Hama, K., Wu, J.-Y., and Heizmann, C.W. (1987). GABAergic neurons containing the Ca2+-binding protein parvalbumin in the rat hippocampus and dentate gyrus. Brain Res. 419, 119-130.

Kubota, Y., Shigematsu, N., Karube, F., Sekigawa, A., Kato, S., Yamaguchi, N., Hirai, Y., Morishima, M., and Kawaguchi, Y. (2011). Selective coexpression of multiple chemical markers defines discrete populations of neocortical GABAergic neurons. Cereb. Cortex 21, 1803-1817.

Lee, A.K., Manns, I.D., Sakmann, B., and Brecht, M. (2006). Whole-cell recordings in freely moving rats. Neuron 51, 399-407.

Nakamura, M., Sato, K., Fukaya, M., Araishi, K., Aiba, A., Kano, M., and Watanabe, M. (2004). Signaling complex formation of phospholipase Cβ4 with metabotropic glutamate receptor type 1α and 1,4,5-trisphosphate receptor at the perisynapse and endoplasmic reticulum in the mouse brain. Eur. J. Neurosci. 20, 2929-2944.

Neddens, J., Fish, K.N., Tricoire, L., Vullhorst, D., Shamir, A., Chung, W., Lewis, D.A., McBain, C.J., and Buonanno, A. (2011). Conserved interneuron-specific ErbB4 expression in frontal cortex of rodents, monkeys, and humans: Implications for schizophrenia. Biol. Psychiatry 70, 636-645.

Nielsen, J.V., Blom, J.B., Noraberg, J., and Jensen, N.A. (2010). Zbtb20-induced CA1 pyramidal neuron development and area enlargement in the cerebral midline cortex of mice. Cereb. Cortex 20, 1904-1914.

Pinault, D. (1996). A novel single-cell staining procedure performed in vivo under electrophysiological control: morpho-functional features of juxtacellularly labeled thalamic cells and other central neurons with biocytin or Neurobiotin. J. Neurosci. Methods 65, 113-136.

Roche, A.E., Bassett, B.J., Samant, S.A., Hong, W., Blobel, G.A., and Svensson, E.C. (2008). The zinc finger and C-terminal domains of MTA proteins are required for FOG-2-mediated transcriptional repression via the NuRD complex. J. Mol. Cell. Cardiol. 44, 352-360.

Schwaller, B., Dick, J., Dhoot, G., Carroll, S., Vrbova, G., Nicotera, P., Pette, D., Wyss, A., Bluethmann, H., Hunziker, W., and Celio, M.R. (1999). Prolonged contraction-relaxation cycle of fast-twitch muscles in parvalbumin knockout mice. Am. J. Physiol. Cell Physiol. 276, C395-C403.

Shigemoto, R., Kinoshita, A., Wada, E., Nomura, S., Ohishi, H., Takada, M., Flor, P.J., Neki, A., Abe, T., Nakanishi, S., and Mizuno, N. (1997). Differential presynaptic localization of metabotropic glutamate receptor subtypes in the rat hippocampus. J. Neurosci. 17, 7503-7522.

Shigemoto, R., Kulik, A., Roberts, J.D.B., Ohishi, H., Nusser, Z., Kaneko, T., and Somogyi, P. (1996). Target-cell-specific concentration of a metabotropic glutamate receptor in the presynaptic active zone. Nature 381, 523-525.
Sloviter, R.S. (1989). Calcium-binding protein (calbindin-D28k) and parvalbumin immunocytochemistry: Localization in the rat hippocampus with specific reference to the selective vulnerability of hippocampal neurons to seizure activity. J. Comp. Neurol. 280, 183-196.
Sylwestrak, E.L., and Ghosh, A. (2012). Elfn1 regulates target-specific release probability at CA1-interneuron synapses. Science 338, 536-540.
Vullhorst, D., Neddens, J., Karavanova, I., Tricoire, L., Petralia, R.S., McBain, C.J., and Buonanno, A. (2009). Selective expression of ErbB4 in interneurons, but not pyramidal cells, of the rodent hippocampus. J. Neurosci. 29, 12255-12264.
Zar, J.H. (1999). Biostatistical analysis, 4 edn (Upper Saddler River: Prentice Hall).